T F A

ACTA FACULTATIS TECHNICAE

TECHNICAL UNIVERSITY IN ZVOLEN

1

ISSUE: XXVI
ZVOLEN 2021

Medzinárodný zbor recenzentov / International Reviewers Board

Mendel University in Brno, Faculty of Forestry and Wood Technology
Alena Očkajová (SK)
Matej Bel University, Faculty of Natural Sciences
Marián Peciar (SK)
Slovak University of Technology in Bratislava, Faculty of Mechanical Engineering
Krzysztof Zbigniew Rokosz (PL)
Koszalin University of Technology, Faculty of Mechanical Engineering
Juraj Ružbarský (SK)
Technical University of Košice, Faculty of Manufacturing Technologies
Ruslan Safin (RU)
Kazan National Research Technological University
Sergey Spiridonov (RU)
State Institution of Higher Professional Education, Saint Petersburg State
Dana Stančeková (SK)
University of Žilina,Faculty of Mechanical Engineering
Vladimír Štollmann (SK)
Technical University in Zvolen, Faculty of Forestry
Marian Šušniar (HR)
University of Zagreb, Faculty of Forestry
Paweł Tylek (PL)
University of Agriculture in Krakow, Faculty of Forestry
Valery Zhylinski (BY)
Belarusian State Technological University

TABLE OF CONTENTS

SCIENTIFIC PAPERS

SCIENTIFIC PAPERS

DEPENDABILITY ANALYSIS OF CRITICAL COMPONENTS OF AN AGRICULTURAL TRACTOR

ANALÝZA SPOĽAHLIVOSTI KRITICKÝCH KOMPONENTOV POĽNOHOSPODÁRSKEHO TRAKTORA

David Fabiánek

Department for Quality and Dependability of Machines, Faculty of Engineering, Czech University of Life Sciences Prague, Kamýcká 129, 165 21, Prague, Czech Republic, fabianekd@tf.czu.cz

ABSTRACT: One of the possibilities of increasing the profitability of machine operation is to optimize its maintenance program. To optimize it, it is important to know dependability of each machine part. This article analysis a vast database containing operation data of 166 agricultural tractors John Deer 7530. The database contains 3262 records. Time period of data acquired data was from 4.1.2010 to 28.5.2019. The maintenance record with the smallest wear and tear that appears in the database is 0 EH (probably a presale preparation of the machine) and the largest 19006 EH. The database contain complete and not complete data, which it means that many of the monitored mechanical parts are in operation state and have not failed. Using critical quantification, 10 critical components were selected. Furthermore, the method of calculation of dependability indicators is described by parametric statistical methods according to ČSN EN 61649:2009 and mean time to operating failure. The Exhaust gas cooler was evaluated as the most critical. The criticality is 1813695.83. Torsional vibration damper seems to be the most suitable for optimizing the preventive maintenance program where the shape parameter α=3.28, the scale parameter β = 11683 and the mean operating time to failure E(t)=10477 EH. The results can be used to optimize the preventive maintenance program and significantly reduce the life cycle costs of the machine.

Key words: dependability, weibull distribution, agriculture, tractor

ABSTRAKT: Jednou z možností zvýšenia ziskovosti prevádzky stroja je optimalizácia jeho programu údržby. Pre jeho optimalizáciu je dôležité poznať ukazovatele spoľahlivosti kritických častí stroja. Tento článok analyzuje rozsiahlu databázu obsahujúcu prevádzkové údaje 166 poľnohospodárskych traktorov John Deer 7530. Databáza obsahuje 3262 záznamov. Časové obdobie vo, ktorom bola prevádzková dáta zaznamenávané je od 4.1.2010 do 28.5.2019. Záznam o údržbe s najmenším opotrebením, ktorý sa v databáze objavil, je 0 Mth (pravdepodobne predpredajnej príprava stroja) a najväčší 19006 mth. Databáza obsahuje úplná a neúplná pozorovania (nedošlo k zlyhaniu skúmaného objektu). Pomocou kvantifikácia kritickosti bolo vybraných 10 kritických komponentov. Ďalej boli vypočítané ich indikátory spoľahlivosti pomocou parametrické štatistické metódy podľa ČSN EN 61649: 2009 a stredná doba do poruchy. Ako najkritickejšie bol vyhodnotený Chladič výfukových spalín. Kritickosť je 1813695,83. Ako najvhodnejšie pre optimalizáciu programu preventívnej údržby sa javí Tlmič torzných kmitov kde parameter tvaru α=3,28, parameter mierky β=11683 a mean operating time to failure E(t)=10477 mth.

Kľúčové slová: spoľahlivosť, weibullovo rozdělení, zemědlství, traktor

INTRODUCTION

At present, manufacturing companies face great pressure from a highly competitive environment and are forced to search new ways to improve production of quality and reduce production costs. (Elmoselhy 2013, Egilmez et al. 2014) Great emphasis is placed on keeping production equipment in high readiness, which generates demanding requirements for their maintenance. By a suitable setting of the maintenance policy, it is possible to significantly extend the operation time until failure, maintenance costs and the life cycle of the production equipment. (Loganathan and Gandhi 2016, Legat 2013).

Significant help in building optimal maintenance programs is the knowledge of dependability indicators. Dependability indicators are:

- Density function of operating time to failure f(t).
- Probability of failure F(t).
- Reliability function R(t).
- Failure rate λ(t). (Legat 2013, Legat et al. 2002, Sherif 1982).

Weibull is very often used to determine dependability approximation. It is very flexible and it can be applied for data modeling without regards to failure tendencies (rising, falling or constant). It is essential to keep track of time of failing, cycles, shipping distance, mechanical stress or similar continuous or discrete parameters (Nassar et al. 2017, Teringl et al. 2015).

This paper demonstrates on 10 critical components of a John Deere 7530 tractor the dependability quantification results obtained using the parameters of the Weibull distribution function which can be an important element in optimizing the tractor maintenance program. The analyzed data are complete in cases in case of complete failure and incomplete in cases where a part did not fail.

MATERIAL AND METHODS

For calculate indicators of dependability a database from STROM Praha a.s. was used. The company is exclusive distributor of JOHN DEERE technology for CZ and also an authorized service. The database consists of 3262 records. The time period in which the maintenance data were acquired is from 4.1.2010 to 28.5.2019. Data were recorded on 166 machines of the same model of agriculture tractor John Deere 7530. The operating hour [EH] is used as a unit of operating time. The maintenance record with the smallest wear and tear that appears in the database is 0 EH (probably a pre-sale preparation of the machine) and the largest 19006 EH.

Critical components were selected by this procedure:

1. Determining the number of occurrences of failures of individual components in the monitored period.
2. Deletion of irrelevant records (objects changed within preventive maintenance programs, work operations, connection of diagnostic devices, etc.).
3. To ensure the usability of the calculated dependability indicators, objects with the number of occurrences of failures <10 were removed from the database.

4. The calculate of average prices of components in the monitored period.
5. The criticality was quantified using the equation:

$$K = n_F \cdot C, \tag{1}$$

Where:
K……criticality
n_F…... number of failures in a given time period (Elmoselhy 2013)
C…… average prices of the components for the period [EUR/ given time]
6. Division of components into three categories according to their criticality using Pareto analysis in the ratio A = 80 %, B = 10 % and C = 10 % of the total cumulative value of the criterion.
7. Selected objects for further research are listed in Table 1.

Table 1 Selected components for research according to criticality
Tabuľka 1 Vybrané komponenty výskumu vzhľadom na kritickosť

Nomenclature of components	Name of the nomenclature	Criticality
RE535729	Exhaust gas cooler	1813695,83
SE502330	Turbocharger	1543399,18
RE537578	Tlumič torzních kmitů	449349,35
RE43738	Tensile force sensor	352457,50
SE501227	Water pump	319146,07
AL160250	Three-way brake valve	304104,34
AL168483	Fuel pump	69313,17
RE543308	EGR valve	2510,23
RE523318	Turbo actuator	2453,77
RE167207	Engine oil pressure sensor	416,62

It should be added that when selecting objects for further research, emphasis was placed not only on their cost criticality, but also on operational criticality. This means that only such objects were selected which, due to their failure, make it impossible to perform the required production tasks. This fact significantly contributes to the total maintenance costs due to the associated cost items, which in the case of a tractor can be, for example, its towing, repair in difficult conditions (accident site), higher purchase price due to express delivery time, or production losses resulting from noncompliance with agrotechnical deadlines. The input data for the calculation of the dependability indicators of individual objects are in Table 2. The table contains operating times until the failure of the object and times without failure, socalled incomplete observations (operating time without failure). Only the data for object RE535729 Flue gas return cooler is given in the article as an example due to the large size of the files.

Table 2 Input data for calculation of object dependability indicators RE535729
Tabuľka 2 Vstupné údaje pre výpočet indikačných faktorov objektu RE535729

Failure number											
Operating time to failure [EH]											
1	2	3	4	5	6	7	8	9	10	11	12
2	1080	1303	1820	1913	2057	2200	2205	2311	2377	2642	2798
13	14	15	16	17	18	19	20	21	22	23	24
2906	2912	2965	2997	3053	3271	3296	3470	3532	3602	3671	3727
25	26	27	28	29	30	31	32	33	34	35	36
3762	3792	3917	3948	4057	4148	4183	4401	4452	4471	4578	4752
37	38	39	40	41	42	43	44	45	46	47	48
4904	4982	5001	5117	5150	5194	5417	5523	5770	5790	5814	5852
49	50	51	52	53	54	54	55	56	57	58	59
6109	6225	6350	6381	6530	6715	6750	6954	7214	7277	7331	7373
60	61	62	63	64	65	66	67	68	69	70	71
7688	7704	8118	8312	8391	8529	8689	8785	8969	8993	9094	9203
72	73	74	75	76	77	78	79	80	81	82	
9363	9461	9938	9987	10440	11281	11299	12229	12300	12804	13458	
Operating time without failure [EH]											
23	135	214	324	357	369	533	583	589	656	700	729
743	819	924	928	944	1001	1004	1007	1187	1244	1324	1385
1405	1412	1428	1442	1543	1647	1746	1872	1933	1940	1972	2119
2251	2625	2646	2797	2814	2816	2905	3033	3051	3057	3084	3088
3142	3213	3244	3255	3311	3317	3467	3503	3539	3541	3576	3655
3719	3757	3780	3782	3983	4041	4095	4218	4320	4333	4345	4368
4425	4435	4498	4511	4602	4683	4762	4789	4833	4849	4913	4946
4980	5094	5300	5337	5380	5474	5523	5854	5918	5927	5928	5945
5962	6007	6066	6112	6196	6247	6262	6395	6429	6497	6499	6500
6600	6604	6884	6965	7060	7125	7335	7346	7435	7578	7674	7706
7836	7932	7962	7988	8055	8132	8219	8413	8431	8549	8570	8625
8721	8798	8901	9200	9380	9386	9444	9495	9540	9803	9956	10141
10848	10904	11293	11300	11527	11781	12095	12326	13388	13427	13713	14160
14212	14844	15170	15790								

The data were processed using the Weibull analysis with the support of an Excel spreadsheet. The analysis procedure was in accordance with the standard ČSN EN 61649:2009.

1. Ascending order of input data
2. Bernard›s approximation

3. Replacement of a modified distribution function *F(t)*
4. Linear regression – linear equation
   a) Calculation of parameter α of shape and β scale of Weibull distribution (Legat et al. 2017).

Furthermore, other dependability indicators were calculated.

1. The Weibull distribution probability density function of operating time to failure

$$f(t) = \frac{\alpha_t}{\beta_t^{\alpha}} \cdot t^{\alpha_t - 1} \cdot exp\left[-\left(\frac{t}{\beta_t}\right)^{\alpha_t}\right] \quad (2)$$

Where:

α_t Shape parameter of Weibull distribution [-],
β_t Scale parameter of Weibull distribution [-],
t Operating time to failure [EH].

2. Reliability function $R(t)$

$$R(t) = exp\left[\left[-\left(\frac{t}{\beta_t}\right)^{\alpha_t}\right]\right] \quad (3)$$

3. Probability of failure $F(t)$

$$F(t) = 1 - exp\left[\left[-\left(\frac{t}{\beta_t}\right)^{\alpha_t}\right]\right] \quad (4)$$

4. Failure rate $\lambda(t)$

$$\lambda(t) = \frac{\alpha_t}{\beta_t} \cdot \left(\frac{t}{\beta_t}\right)^{\alpha_t - 1} = \frac{f(t)}{R(t)} \quad (5)$$

5. Mean Operating Time to Failure $\mathrm{E}(t) = MOTTF$

$$MOTTF = \beta \cdot \Gamma\left(1 + \frac{1}{\alpha}\right) \quad (6)$$

When calculating the MOTTF in MS Excel, it is necessary to use the formula for the Γ - GAMMA function.

RESULTS AND DISCUSSION

No dependability analysis performed on similar components from same the agriculture machine monitored for so long time as presented in this article was found in the available literature. There is nothing to compare the results with. From the point of view of the conditions in which the production processes of these branches are realized and from the point of view of the composition of production equipment, a completely new discipline

opens up for research activities – operational dependability and optimization of renewal, which must be given due attention and help practice. Dependability indicators of selected components are in tables Table 3. Dependability characteristics *F(t), f(t), R(t), λ(t)* for calculated Weibull distribution for RE535729 Exhaust gas cooler are in Fig. 1

Table 3 Weibull distribution parameters, indicators of dependability
Tabuľka 3 Weibullove distribučné parametre, indikátory spoľahlivosti

Machines component		α shape parameter	β scale parameter	E(t) [EH]
RE535729	Exhaust gas cooler	1,47	13601	12313
SE502330	Turbocharger	1,43	35137	31936
RE537578	Torsional vibration damper	3,28	11683	10477
RE43738	Tensile force sensor	0,86	36663	39585
SE501227	Water pump	2,86	14739	13136
AL160250	Three-way brake valve	0,71	113460	141273
AL168483	Fuel pump	2,58	22919	20351
RE543308	EGR valve	1,06	57135	55784
RE523318	Turbo actuator	2,00	23413	20749
RE167207	Engine oil pressure sensor	2,03	21374	18937

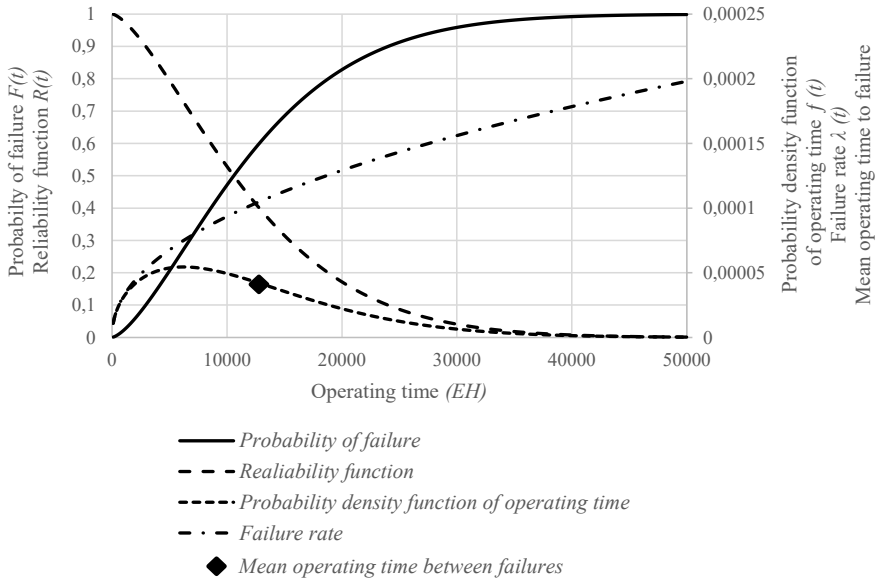

Fig. 1 Dependability characteristics *F(t), f(t), R(t), λ(t)* for calculated Weibull distribution for RE535729 Exhaust gas cooler
Fig. 1 Charakteristiky závislostí *F(t), f(t), R(t), λ(t)* pre výpočet Weibullovho rozdelenia pre Chladič výfukových plynov RE535729

CONCLUSION

One of the ways to increase the profitability of machine operation is to optimize its maintenance program. Therefore, to optimize the program, it is necessary to know the dependability data of individual machine components. In this paper, an extensive database containing data on the operation of 166 agricultural tractors of the same model was analyzed. Using critical quantification, 10 critical components were selected. The calculated dependability indicators using equations 2–6 applied to the collected operating data of selected tractor components indicate that further research into the application of statistical methods to optimize the maintenance program of selfpropelled production equipment makes sense. Among the critical components of the tractor, there are those in which the results of the failure characteristics indicate that the increase in failure intensity is not accidental in nature. However, this hypothesis needs to be confirmed by further research. The Exhaust gas cooler was evaluated as the most critical. The criticality is 1813695.83. Torsional vibration damper seems to be the most suitable for optimizing the preventive maintenance program where the shape parameter $\alpha = 3.28$, the scale parameter $\beta = 11683$ and the mean operating time to failure $E(t) = 10477$ EH. The results can be used to optimize the preventive maintenance program and significantly reduce the life cycle costs of the machine.

LITERATURE

CSN EN 61649 (010653). (2009). Weibull analysis (In Czech).

EGILMEZ, G., ERENAY, B., SÜER, G. 2014. Stochastic skill-based manpower allocation in a cellular manufacturing system. Journal of Manufacturing Systems 33(4), pp 578–588.

ELMOSELHY, S., 2013. Hybrid lean–agile manufacturing system technical facet, in automotive sector. Journal of Manufacturing Systems 32(4), pp 598–619.

LEGAT, V., MOSNA, F., ALES Z. JURCA, V., 2017. Preventive Maintenance Models – Higher Operational Reliability. Eksploatacja I Niezawodnosc-Maintenance and Reliability 19(1), pp 134–141.

LEGAT, V., 2013. Management and maintenance engineering. Professional Publishing.

LEGAT, V., MOSNA, F., CERVENKA, V., JURCA, V. 2002. Optimization of preventive maintenance and information system. Eksploatacja i Niezawodność., 4(16), pp 24–29.

LOGANATHAN, M., GANDHI, O. 2016. Maintenance cost minimization of manufacturing systems using PSO under reliability constraint. International Journal of System Assurance Engineering and Management 7(1), pp 47–61. DOI:10.1007/s13198-015-0374-2.

NASSAR, M. A., ALZAATREH, M., ABO-KASEM, O., 2017. Alpha power Weibull distribution. Communications in Statistics – Theory and Methods, pp 1–17.

SHERIF, Y. 1982. Optimal maintenance schedules of systems subject to stochastic failure. Microelectronics Reliability 22(1), pp 15–29. DOI:10.1016/0026-2714(82)90047-6.

TERINGL, A., ALEŠ, Z., LEGÁT, V. 2015. Dependability characteristics – indicators for maintenance performance measurement of manufacturing technology. Manufacturing Technology 15(3), pp 456–461. DOI:10.21062/ujep/x.2015/a/1213-2489/mt/15/3/456.

Corresponding author:
David Fabiánek, tel. 605133898, e-mail: fabianekd@tf.czu.cz

APPLIED RESEARCH IN THE FIELD OF FOREST FIRES USING EXISTING FORESTRY EQUIPMENT

APLIKOVANÝ VÝSKUM V OBLASTI LESNÝCH POŽIAROV PRI VYUŽITÍ EXISTUJÚCEJ LESNEJ TECHNIKY

Matej Priatka[1], Michaela Hnilicová[2], Ivan Chromek[3], Richard Hnilica[4]

[1] Department of Forest Harvesting, Logistics and Ameliorations; Faculty of Forestry; Technical University in Zvolen; T.G. Masaryka 24, 960 01 Zvolen, Slovak Republic
[2] Department of Mechanics, Mechanical Engineering and Design; Faculty of Technology; Technical University in Zvolen; T.G. Masaryka 24, 960 01 Zvolen, Slovak Republic
[3] Department of Fire Protection; Faculty of Wood Sciences and Technology; Technical University in Zvolen; T. G. Masaryka 24, 960 53 Zvolen, Slovak Republic
[4] Department of Manufacturing Technology and Quality Management; Faculty of Technology; Technical University in Zvolen; T.G. Masaryka 24, 960 01 Zvolen, Slovak Republic

ABSTRACT: The forest wheeled skidder has been developed from its beginnings as a single-purpose machine for the needs of skidding in the forest. The essence of the technical solution of the fire adapter is to ensure the transport of a sufficient amount of water with the necessary equipment to ensure fire-fighting conditions of mountain forests. The proposed construction of the fire adapter will be adapted to the parameters of the LKT base machine on which the adapter will be carried. The paper deals with the analysis of input factors that predispose this type of construction to ensure the transport of water supply in case of fire brigades in forest fires. The input factors for the use of LKT mainly include analysis of the terrain, which is capable of this type of equipment to move, analyze the appropriateness of placing the adapter for the transport of water, the selection of appropriate materials, design and construction solutions. The aim of these analytical procedures is to conservation the original features and to extend the target use of special machines.

Key words: fire, forest wheeled skidder, adapter, slope gradient, forest

ABSTRAKT: Lesný kolesový ťahač bol od svojich začiatkov vyvinutý ako jednoúčelový stroj pre potrebu približovania dreva v lesnom prostredí. Podstatou technického riešenia protipožiarneho adaptéra je zabezpečenie dopravy dostatočného množstva vody s nevyhnutnou výbavou pre zabezpečenie hasenia požiaru v podmienkach horských lesov. Navrhnutá konštrukcia protipožiarneho adaptéra bude prispôsobená parametrom bázového stroja LKT, na ktorom bude adaptér nesený. Príspevok sa zaoberá analýzou vstupných faktorov, ktoré predurčujú tento typ technického prostriedku k využitiu pre zabezpečenie dopravy vody v prípade zásobovania hasičských jednotiek pri lesnom požiari. K týmto faktorom patrí rozbor terénu, v ktorom je schopný tento typ techniky sa pohybovať, analýza vhodnosti umiestnenia adaptéra pre dopravu vody, výber vhodných materiálov, dizajnu a konštrukčných riešení. Cieľom týchto analytických postupov je zachovanie pôvodných vlastností a rozšírenie cieľového využitia tohto jednoúčelového stroja.

Kľúčové slová: požiar, lesný kolesový ťahač, adaptér, sklon, les

INTRODUCTION

Ongoing climate change and its consequences are often discussed in professional circles as the main cause of future increased frequency of natural disasters, including fires in the natural environment. Climate change affects forest fires directly through weather conditions, which influence the onset and spreading of fire, and indirectly through its impact on vegetation and combustible material. It is assumed that the risk of fire occurrence in Europe will increase with the most extreme fires occurring more frequently, which destroy vast areas and have long-term consequences. Results of studies on fires, which occurred in the European continent in the last 30 years, show an increase in the duration of a fire season and it is assumed that a fire regime will change almost everywhere across Europe. While the total area in the South European countries destroyed by fire is increasing each and every year, northern areas like Scandinavia are afflicted by unprecedented forest fires. Due to global warming and increasing aridity, the risk of increased frequency and extent of wildfires is very high. Many regions of the world have experienced an increasing trend of excessive wildfires and an increasing occurrence of extremely severe fires (FAO Fire management 2006). The total area of forest fires in the EU over the last 20 years has been around 8.7 million hectares, with an annual average of around 415,000 hectares. The most extensive fires were recorded in 2000, 2003, 2005, 2007, 2012 and 2017. The fires in these years were above the annual average. (San-Miguel-Ayanz et al. 2020) In 2017, wildfires burnt be around 1 million hectares of natural lands in the EU. The European Forest Fire Information System estimated the amount of fire-related losses to be around 10 billion Euros (San-Miguel-Ayanz et al. 2018).

Forest fires in Slovakia often occur in the areas inaccessible to fire-fighting machinery with insufficient or rather inadequate water supply for fire-fighting purposes. The facts provided above are based on statistically processed data on fire in state forests of the Slovak Republic in the last ten years. The results are presented in the Figures 1 and Table 1.

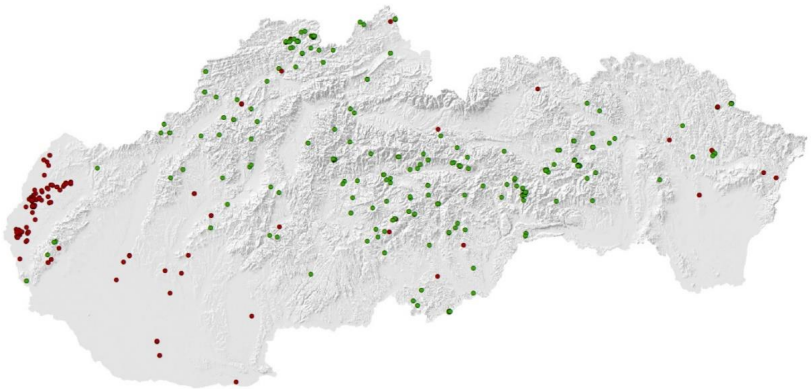

Fig. 1 Map of fires in state forests of the Slovak Republic in 2010 – 2020 (Lesy SR)
red marks – fires in the terrain with a slope until 16%
green marks – fires in the terrain with a slope over 16%

According to these results, there can be concluded that the greatest damage is caused by fires in the forests of the Slovak Republic at a slope gradient of 16%. As a result, our research was aimed in this direction.

Tab. 1 Fires in state forests of the Slovak Republic in 2010 – 2020

slope gradient	forest fire (2010 – 2020)			
	number	duration [h]	fire-affected area [ha]	financial loss [Eur]
until 16%	133	444	95,4	211 063,45
over 16%	195	2723	452,5	927 373,93

Elimination of forest fires, any scale combines several phenomena. Firstly, sufficient forces and resources for its localization and liquidation. Secondly, the availability of the site and sufficient extinguishing agent (water) in connection with the availability of water resources themselves. Not one area of this vicious circle can´t be prepared in advance. However, making the forest accessible with the preservation, revitalization and construction of the forest road network and water resources should be part of the construction of the forest. All this in accordance with the preservation of production and increasingly presented non-production functions of the forest. (Chromek et al. 2017)

It is necessary to look at safety construction from the point of view that it is not just a question of designing and dimensioning machinery, but the creation of a comprehensive system of filling defined objectives. This means that for adapters, which are used as attachments forestry machinery, it is necessary to approach the design from two perspectives. The first is the purpose for which the adapters are designed (operational characteristics) and the second is the impact on the operator or other employees working nearby. The task of designers who deal with technical (operational) parameters is to ensure the highest possible efficiency of the machine with the adapter. The role of engineers who deal with security, is to minimize the hazards arising throughout the life of the machine (Hnilica et al. 2015; Wiesik & Aniszewska 2011).

Design and development of pumping appliance (CAS) for fire-fighting in inaccessible forest fire areas collides with high costs from point of view of development, and also with limited possibilities of mass production (piece production). The last question is utilization of such a one-purpose machine, mainly number of uses in relation to working life of the machine. This is the basic problem, that creates a room for alternative solutions. In this paper the solution is based on analysis of the terrain in which the machine operates, selection of a machine that exists in present, and is suitable for this environment, design of a body – adapter, based on water tank, selection of suitable materials from point of view of strength and low weight. Another criterion is a shape of the water tank with accent on conservation of native travel abilities of the base vehicle.

MATERIAL AND METHODS

The need to transport water nearest the intervening fire brigade has become a basic hypothesis at the thought of a suitable design of the fire equipment. Based on this hypothesis, the most appropriate alternative treatment and the use of forest machinery. The starting point for the design will be the definition of the body carrier with maximum provision of slope accessibility and permeability in forest terrain. The starting point for the design will

be the definition of the body carrier with maximum provision for slope accessibility and workability in forest terrain. Another important criterion will be the use of available technique (base machine) used in forestry, without the need to intervene in its construction, eventually the development of new technique. When accepting the basic requirements in relation to workability in forest terrain, forest wheeled skidders (LKT) came into consideration as base machines. These base machines are primarily designed and intended to work in difficult forest terrain.

The main task of LKT is to move wood from the forest to the place of further manipulation. In the case of a transport of an extinguishing agent, it is a change of the basic working algorithm. The space remains, the direction of movement changes only. For this reason, when considering how to use existing LKT for these purposes, the design of the fire-fighting adapter will be based on the following basic concepts of its use:

- the use of base machine (LKT) in the form of a pulling device to increase the CAS's accessibility – concept I (Fig. 2a),
- the use of base machine (LKT) as a pulling device for pulling a one-axle or two-axle trailer – concept II (Fig. 2b),
- the use of base machine (LKT) as a carrier for the transport of water (a special purpose machine) – concept III (Fig. 2c),
- the use of base machine (LKT) as a carrier for a removable water transport body – concept IV (Fig. 2d).

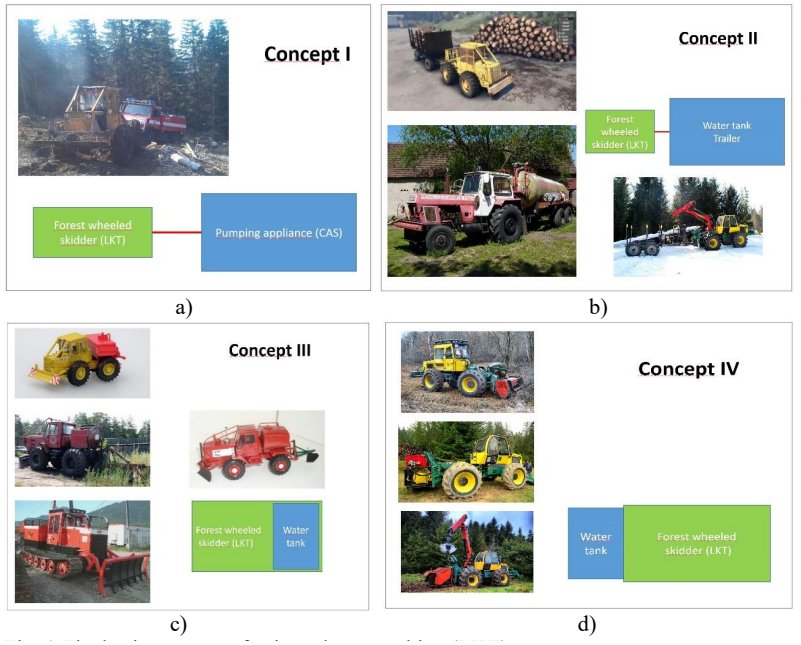

Fig. 2 The basic concept of using a base machine (LKT)
a) in the form traction gear to increase the endurance distance of CAS
b) in the form traction gear to increase a one-axle or two-axle trailer (MUDRUNNERMODS)
c) as a carrier of a fixed body for water transport – a special purpose machine (KMC Kootrac; HO-MODELY)
d) as a carrier of detachable body for water transport

As it can be seen from concept I, LKT is used as a traction device to increase the uptake of fire-fighting equipment in the forest terrain. In this case, it could be pulled by LKT, e.g. MB UNIMOG CAS (Fig. 2a). However, this solution is at the limit of the possibility of this technique with the risk of its damage.

Concept II hits a limited capability of the trailer, in relation to its stability (Fig. 2b) when crossing the terrain (churning up the road, the tracks on the road, the stones or the root stones and the tires).

The concept III shows the uniqueness of such a machine (Fig. 2c), which significantly increases the costs of its production and operation. Small-scale or piece production does not ensure its presence in the area, in the event of a forest fire.

Under concept IV, the original purpose of LKT is preserved, with minimal constraints on driving characteristics (Fig. 2d). With a volume of carried fire-extinguishing material, approx. 2000l replaces vehicles based on P V3S or MB UNIMOG chassis. In this way, the original LKT function is retained with minimal delay when applying the body to the rear LKT shield.

Fig. 3 The use of a base machine in fires in the forest, as a carrier of a detachable body

When designing an alternative location adapter (body) was based on two options. Design of a special platform for the rear axle LKT, or an adapter for the rear LKT shield. After considering all the pros and cons, the adapter was developed, using the rear LKT shield. (Fig. 3).

RESULTS AND DISCUSSION

Based on concept IV, we approached the technical solution of the fire-fighting adapter for LKT, specifically the selection of adequate construction materials with requirements for their strength and minimum weight. The basic condition for the design of the adapter is the use of the reserve of the capacity weight of the base machine with emphasis on:

– the center of gravity of the vehicle, depending on the change in driving characteristics,
– strength characteristics of the materials used for each part of the adapter,
– design and draft of the dimensions of the adapter, with respect to the dimensions of the attachment point,

– design of a water tank with a minimum water volume of 2,000 L (based on the useful load capacity of LKT and the requirements of the fire brigade),
– design and draft of breakwaters in the tank,
– design of the protective frame of the tank.

The design of the fire-fighting adapter must be adapted to the parameters of base machine LKT. The LKT will be carried on the inclinable rear log arch. The fire-fighting adapter must also be able to be transported on other means, so it can be dismantled. The proposed fire-fighting body with its equipment will meet the criteria for forest fire interventions and monitoring of forest area.

The basic technical parameters for the fire-fighting adapter on LKT will be:
– water volume of about 2,000 L,
– fire-fighting adapter equipment (high-pressure motor pump, fire extinguishing box),
– anchorage of the fire-fighting adapter on the inclinable rear log arch,
– the protective frame that ensures fire-fighting adapter handling (tank transfer, tank lifting),
– independent extinguishing after disconnecting the base-machine,
– possibility of transportation of parts to build a lake system of water relay of forest fires-fighting.

The gradient of up to 16% allows for a faster intervention even with the existing technology. These conditions enable a fast transportation of the extinguishing agent (water) to the place of intervention. Requirements for the accessibility of fire-fighting equipment increase with the terrain gradient rising over 16%, which stems from its technical design. This, in turn, leads to a slower distribution of water to the places requiring intervention.

Considering their construction and use, LKT base machines with hydrostatic energy transmission are suitable for driving adapters for the mechanisation of work in the cultivation and protection of the forest. However, basic forestry-technical requirements for designing adapters should be considered, too. In particular, cost-effectiveness, extensive applications under different conditions, easy and fast installation on LKT, optimum distribution width, operation by the tractor driver from the cab, provision of drive slip in case of fixed obstacles, adequate noise levels, the minimal transmission of vibration to the operator (driver), utilisation of domestic construction and spare parts, components and materials, ecological suitability, sufficient level of occupational safety and health protection as well as sufficient performance. (Hnilicová et al. 2018[a]; Hnilicová et al. 2018[b])

Because the proposed fire-fighting body is to be used in the complicated terrain of mountain forests, its weight must be monitored in its design. Weight is a basic condition for ensuring good stability of the whole machine with an adapter. By reducing the weight, we could achieve better stability of the base machine. Stability, in the case of increased slope navigation or maneuvering on a slope could be increased by placing the adapter on the floor. In this case, it was necessary to use the floating position of the rear LKT shield. In order to increase the capacity weight of the base machine, but also to ensure maximum handling, a four-member operator was therefore applied for the lightweight construction of tanks of composite materials (fiberglass). (Hnilicová & Hnilica 2017)

For reason of transport safety and prevention of vertical and horizontal movement of water in the water tank during transport, as shown in Figure 4, we considered the construction of internal wave-breaks. These breakwaters are part of the construction of the

water tank itself, thereby increasing its overall strength. To simplify maintenance has been undertaken to construct a removable lid.

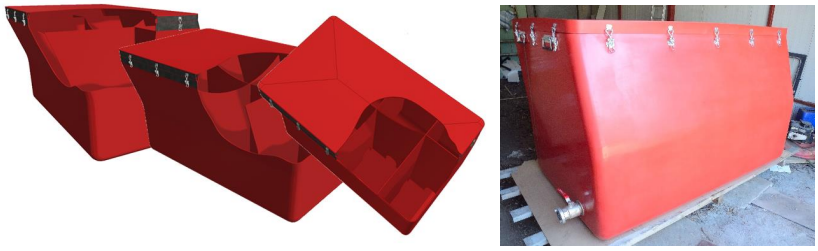

Fig. 4 The water tank construction with built-in wave-breaks

Requirements for the transport of the tank in the forest terrain and the possibility of its damage required the structure of the protective frame (Fig. 5), which performs a protective function during transport, but also when manipulation the water tank outside the transport. In addition, in an emergency, it can serve as an improvised trailer for transporting materials in difficult terrain. In this case, a composite tank is removed from the protective steel frame.

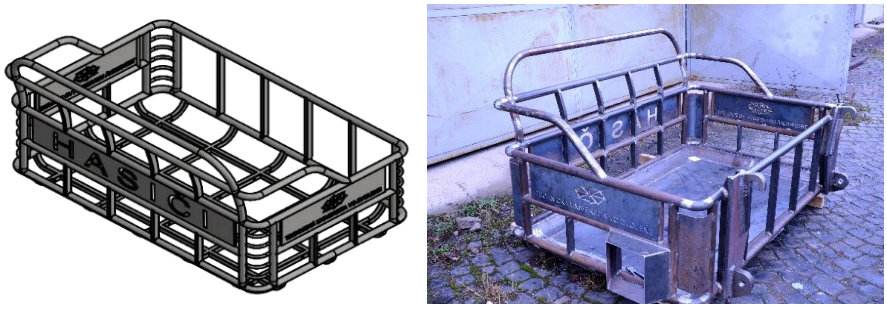

Fig. 5 The protective frame construction of the tank for transporting water

Scheme supporting frame firefighting adapter were processed in Autodesk Inventor using the Shape Generator. This tool represents a new form of computer-aided structural design that provides capabilities beyond classical optimization. It is based on a generative design simulates the natural evolutionary approach. Using a generic design does not result in one solution but a potentially large number (Autodesk, 2017). The created structure is discontinuous and cannot fulfill its their function in the generated state. The built-in algorithm detracts from the generated shape until completion of a specified criterion of weight loss. When replacing such a shape with a real construction, we will not directly arrive at an acceptable design (Fig. 6).

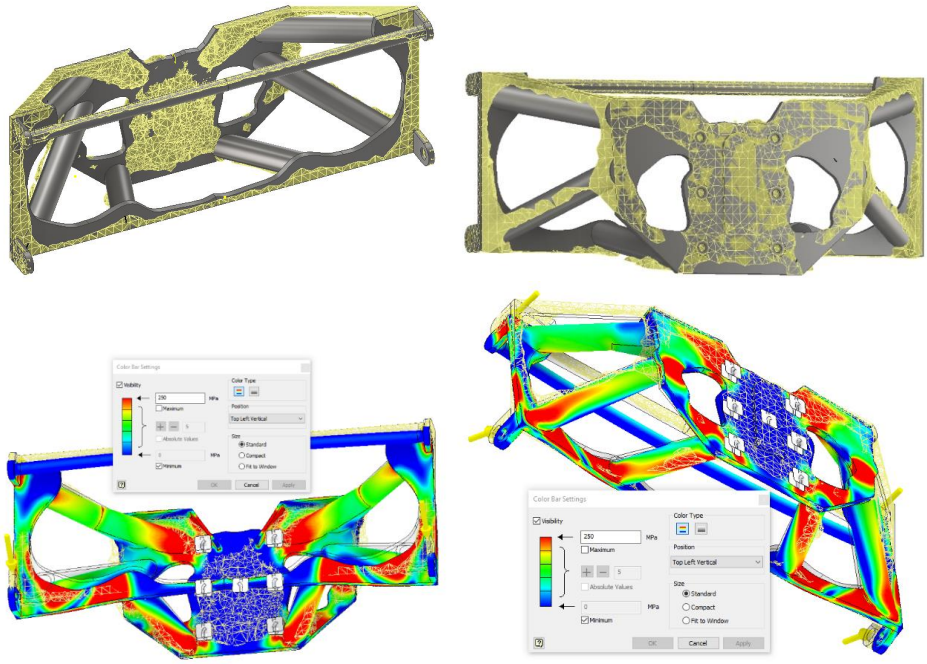

Fig. 6 Replacement of the generated shape by a real construction – the maximum stress significantly by above the stress displayed

To adjust the input form design, we therefore decided to reinforce the structure on the results of regular stress analysis. We designed and applied several reinforcements (Fig. 7) and performed a stress analysis (Fig. 8). Due to the above-mentioned complex theoretical assumptions, we calculated a load of 50 kN, while the weight of the complete body, including the full tank is less than 2,400 kg. This compensates for the fact that even if the device is not designed for dynamic driving, dynamic effects may occur.

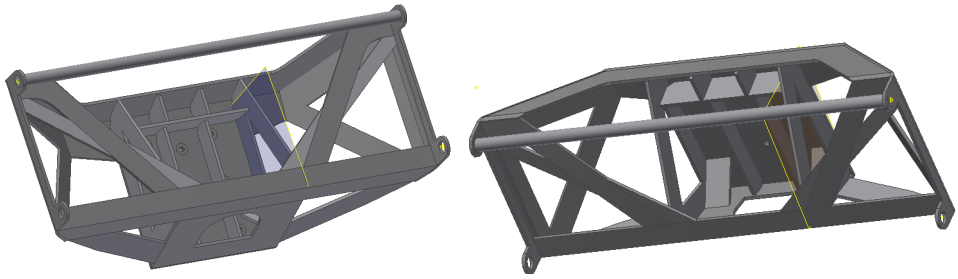

Fig. 7 Modifying the supporting frame

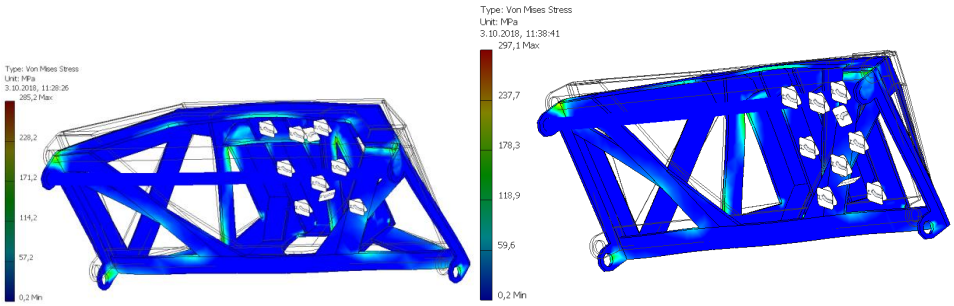

a) b)

Fig. 8 FEA analysis
a) for slope gradient 0 %
b) for slope gradient of 20 % – driving uphill

The basic essence of the technical solution of the fire-fighting adapter is to ensure sufficient water transport with the necessary firefighting equipment for firefighting purposes in conditions of mountain forests. The resulting technical solution of the fire-fighting adapter (Fig. 9) is adapted to the parameters of the base machine LKT, on which the adapter is supported, resp. semi-mounted (floating position) on the rear LKT shield. The adapter can be removed and transported by other means of transport to the place of intervention.

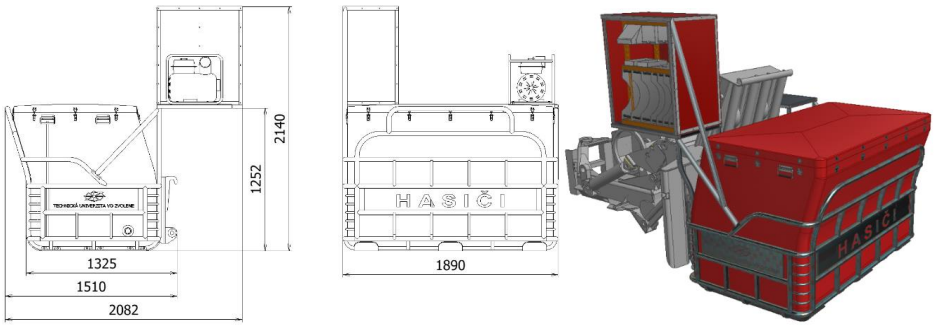

Fig. 9 The design of the fire-fighting adapter

Additional equipment of the fire-fighting adapter to the demands of accepted practice:
- water pump,
- 2“ suction hose (length 125 cm),
- 2” suction hose with strainer (length 250 cm),
- hose “C” (fire hose with connector) 3x20 m,
- hose “D” (fire hose with connector) 4x20 m,
- dividing breeching C – DCD,
- hand branchpipe (“C” Profi, “D” Profi),
- ball valve “C” with connectors,
- the ax-hoe, the spade and the shovel.

This equipment is intended to ensure an autonomous capacity to refill the tank of fire-fighting adapter from the nearest natural water source, as well as to manage the intervention itself in a complicated terrain.

Fire adapter (Fig. 10) its technical design allows transport of water into the area of fire and firefighting forest fires in connected to the base machine LKT. It has an autonomous drive (own motor pump) for filling from a water source and to supply a hose, offensive line. This ensures its full functionality even after disconnecting the base machine LKT.

Fig. 10 Fire-fighting adapter

Besides being used for fighting forest fires, the fire-fighting adapter can also be used for transport of water to forest nurseries (irrigation), freshly planted areas in the event of prolonged drought, filling of watering-places for forest animals and filling puddles in the dry season and cleaning of culverts.

In conclusion, the statistically processed results of operating tests show that the deployment speed of the fire-fighting adapter from its import to intervention is relatively short. Time depends to a large extent on the volume of loaded extinguishing agent. Of course, the delay increases with a full tank. LKT travels 100 m distance with a full tank (2,000 L) in 3 mins 37 secs, while LKT loaded with 1,000 L of extinguishing agent travels the same distance in 2 mins and 16 secs.

Results of slope gradient have shown a difference in the transport of the fire-fighting adapter with a full and half-full tank. It can be said that the time of the adapter deployment increases with a volume of extinguishing agent in a tank and depends on a gradient and distance. Slope gradient limits of the adapter for the purpose of our measurements can be deduced from operating measurements. The adapter attached to LKT riding with a full tank has had a slope gradient limit of 30 %. In the case of a half-loaded tank, it can be said that LKT has a slope gradient limit of 40 %. Operating tests, observations, and consultations with LKT operators have been a prerequisite for improving these parameters. This follows from the technical and performance specifications of base machine LKT. Counterweight installed on the front blade for example in the form of a 500 L tank could improve the stability of a base machine when riding up the slope. It was assumed that the front axle had been lifted at limited gradients and therefore its centre of gravity was displaced. This issue is currently being worked on together with subsequent tests right under operating conditions.

CONCLUSION

At present, the representation of base machines of the LKT type predominates in the forests of the Slovak Republic, but do not have a similar extension, introduced in the present article. Based on the above analysis, it would be appropriate to prepare a proposal on the basis of which a fire-fighting adapter of the said construction would be incorporated into the vehicle fleet. The adapter can be quickly mounted on a LKT base machine, which creates an effective tool in extinguishing fires, especially in inaccessible terrain.

Fire-fighting adapter DATEFF its construction and speed of deployment predestined for liquidation of forest fires in difficult terrain conditions in the forests of the Slovak Republic. At present, when forest fires occur, it is often quite complicated, in forest conditions, to provide sufficient technical support for the rapid prevention and elimination of fires. This fact is largely eliminated by the proposed fire-fighting adapter.

The technical solution was based on the requirement to provide sufficient technical support in difficult terrain conditions for water transport logistics in order to quickly prevent the spread and destruction of forest fire. This adapter is designed for forest wheel tractors that reach 40% slope availability, are able to work on the stand area, overcome obstacles and are available in sufficient quantities in all forest owners. In conclusion we can say that fire adapter DATEFF its parameters meet the above requirements.

ACKNOWLEDGMENT

This work was supported by "Agentúra na podporu výskumu a vývoja MŠVVaŠ SR" under the grant number APVV-14-0468

LITERATURE

AUTODESK: Generative design. 2007. [online] [cit. 2021-03-29] https://www.autodesk.com/solutions/generative-design

FAO Fire management: Review of international cooperation. Fire Management Working Paper FM18E. 2006. [online] [cit. 2021-04-14] https://www.fao.org/3/j9406e/j9406e00

HNILICA R., MESSINGEROVÁ, V., STANOVSKÝ, M., SLUGEŇ, J., HNILICOVÁ, M., FERENČÍK, M. 2015. Možnosti mechanizácie prác pri zakladaní a výchove lesa. Vedecká monografia. Technical university in Zvolen, Slovak Republic, 2015; pp. 99.

HNILICOVÁ, M., HNILICA, R. 2017. Využitie kompozitných materiálov za účelom zníženia hmotnosti nadstavieb pre bázové stroje. In Kvalita, technológie, diagnostika v technických systémoch. SPU Nitra, Slovak Republic, 2017; pp. 69-74.

HNILICOVÁ, M., HNILICA, R., DADO, M., MESSINGEROVÁ, V. Innovative use of forest wheeled skidder for liquidation undesirable advance growth and prevention against fire. Current issues in forests protection from fires – peer-reviewd international proceedings. 2018[a], 40-44.

HNILICOVÁ, M., DADO, M., HNILICA, R., MESSINGEROVÁ, V. Innovative use of the rotary cultivators then adapter forest wheeled skidders. Current issues in forests protection from fires – peer-reviewd international proceedings. 2018[b], 53-57.

HO-MODELY. [online] [cit. 2021-04-14] https://www.ho-modely.cz/product-sk/hasici/hasici-model/lkt-81-turbo-pozarni-pro-haseni-les_poza/264

CHROMEK, I., HNILICA, R., HNILICOVÁ, M., MESSINGEROVÁ, V. 2017. Funkčné nadstavby, jeden zo spôsobov zvýšenia efektívnosti dostupnej techniky pri hasení lesných požiarov. In Požární ochrana 2017: sborník přednášek XXVI. ročníku mezinárodní konference pod

záštitou primátora města Ostravy a Českého národního výboru CTIF – Ostrava, Czech Republic, 2017; pp. 85-87.
KMC-Kootrac. KMC Fire Tracker. [online] [cit. 2021-04-14] https://www.kmc-kootrac.com/remanufacture/firetruck
Lesy SR, š.p. Mapa požiarov 2010 – 2020.
MUDRUNNERMODS. [online] [cit. 2021-04-14] http://www.mudrunnermods.com/?s=LKT
SAN-MIGUEL-AYANZ, J., DURRANT, T., BOCA, R., MAIANTI, P., LIBERTÀ, G., ARTES-VIVANCOS, T., OOM, D., BRANCO, A., DE RIGO, D., FERRARI, D., PFEIFFER, H., GRECCHI, R., NUIJTEN, D., LERAY, T. 2020. Forest Fires in Europe, Middle East and North Africa 2019. Publications Office of the European Union 2020; pp. 164. doi:10.2760/468688
WIESIK, J., ANISZEWSKA, M. 2011. Urzadzenia Techniczne w produkcji lesnej. SGGW, Warszawa, Poland, 2011; pp. 237-240.

Corresponding author:
Michaela Hnilicová, +421-45-52066876, michaela.hnilicova@gmail.com

DESIGN OF HEATER OF COOLANTS FOR EXPERIMENTAL RESEARCH ON THERMAL PARAMETERS IN AUTOMOBILE RADIATORS

NÁVRH OHREVNÉHO TELESA CHLADIACICH KVAPALÍN PRE EXPERIMENTÁLNY VÝSKUM TEPELNÝCH PARAMETROV AUTOMOBILOVÝCH CHLADIČOV

Marek Lipnický[1], Zuzana Brodnianská[2], Pavol Koleda[3]

[1]Department of Environmental and Forestry Machinery, Faculty of Technology, Technical University in Zvolen, Studentska 26, 960 01, Zvolen, Slovak Republic, xlipnicky@tuzvo.sk
[2]Department of Environmental and Forestry Machinery, Faculty of Technology, Technical University in Zvolen, Studentska 26, 960 01, Zvolen, Slovak Republic, zuzana.brondianska@tuzvo.sk
[3]Department of Manufacturing and Automation Technology, Faculty of Technology, Technical University in Zvolen, Studentska 26, 960 01, Zvolen, Slovak Republic, pavol.koleda@tuzvo.sk

ABSTRACT: The paper focuses on the design and optimization of a heating element for coolants in the experimental cooling circuit of a Skoda Fabia 1.4 MPI. The experimental set up is intended for research of car radiators, their thermal parameters and used coolants in laboratory conditions. The cooling circuit of the assembly consists of a motor model, connecting pipes, a radiator with a fan, an electric motor of a water pump and a heating element. Since the engine model does not burn and thus does not generate any heat from the combustion chamber, the heat is generated by the heater. The operating temperature of the coolant to be reached by the heater is 80 to 90 °C, depending on the type of thermostatic valve used. The volume of coolant in the experimental set is 6l. The paper presents a gradual design of the heating element, which underwent changes and optimization (variants 1 to 3) to achieve real operating parameters of flow and heating time of coolants, and their smoother flow through the heating element. The third variant of the manufactured heating element best suits the experimental conditions even under long-term loading. Its shape was designed with a circular cross-section ø 80 mm to achieve a cooling circuit volume specified by the manufacturer of 5.6l. The designs of radiators are also compared and presented in the form of three-dimensional models in Creo Parametric 7.0.1.0. The proposal is based on theoretical and practical knowledge in the field.

KEYWORDS: Engine cooling circuit, car radiator, heater, coolant, Skoda Fabia.

ABSTRAKT: Príspevok je zameraný na návrh a optimalizáciu ohrevného telesa chladiacich kvapalín v experimentálnom chladiacom okruhu vozidla Škoda Fabia 1.4 MPI. Experimentálna zostava je určená na výskum chladičov automobilov, ich tepelných parametrov a použitých chladiacich kvapalín v podmienkach laboratória. Chladiaci okruh zostavy pozostáva z modelu motora, spojovacích potrubí, chladiča s ventilátorom, elektromotora vodného čerpadla a ohrevného telesa. Vzhľadom k tomu, že model motora nespaľuje, a teda nevytvára žiadne teplo od spaľovacieho priestoru, teplo je generované ohrevným telesom. Pracovná teplota chladiacej kvapaliny, ktorú je potrebné dosi-

ahnuť ohrevným telesom, má hodnotu 80 až 90 °C v závislosti od typu použitého termostatického ventilu. Objem chladiacej kvapaliny v experimentálnej zostave je 6 litrov. V príspevku je uvedený postupný návrh ohrevného telesa, ktorý prechádzal zmenami a optimalizáciou (variant 1 až 3) pre dosiahnutie reálnych prevádzkových parametrov prietoku a času ohrevu chladiacich kvapalín, a ich plynulejšieho prúdenia cez ohrevné teleso. Tretí variant zhotoveného ohrevného telesa najviac vyhovuje experimentálnym podmienkam aj pri dlhodobom zaťažení. Jeho tvar bol navrhnutý s kruhovým prierezom ø 80 mm pre dosiahnutie objemu chladiaceho okruhu stanoveného výrobcom 5,6 l. Návrhy ohrevných telies sú porovnané a prezentované aj formou trojdimenzionálnych modelov v Creo Parametric 7.0.1.0. Návrh vychádza z teoretických a praktických poznatkov v danej problematike.

KĽÚČOVÉ SLOVÁ: Chladiaci okruh motora, automobilový chladič, ohrevné teleso, chladiaca kvapalina, Škoda Fabia.

INTRODUCTION

The issue of heat transfer in terms of energy savings, or efficient cooling, is a topic, nowadays. Research of heat exchange systems in terms of geometric and physical parameters is important and their optimization significantly affects the more efficient heat exchange process. Internal combustion engine cooling plays a significant role in the engine›s heat balance, as it dissipates about a third of the heat supplied to the engine. When the mixture is burned, high temperatures are generated in the combustion chamber (up to 2200 °C). As combustion alternates with the suction of mostly cold mixture, the overall engine temperature is lower. In order to maintain the optimum operating temperature of the engine from 80 °C to 90 °C and the constantly changing mechanical properties of the individual engine components when a certain temperature limit is exceeded, cooling is necessary. In terms of continuous thermal stress, the motor needs an additional device – a heat dissipation system. In automobiles, the purpose of the engine cooling system is to dissipate the excess heat generated during the combustion process and transferred to the individual engine parts and also to the engine oil.

The authors› experimental set (Hussein et al. 2014) included a plastic tank, electric heater, centrifugal pump, flow meter, pipes, valves, direct current source, ten T-type thermocouples for temperature measurement and a heat exchanger (car radiator). An electric heater with a power of 1500 W was installed inside a plastic tank / bucket (height 400 mm and diameter 300 mm). It was used instead of the engine - combustion process to heat the flowing liquid. The voltage regulator (0 - 220V) was used to supply energy and regulate the temperature in the radiator (60 - 80 ℃). The pipes connecting the heater to the radiator are 12.7 mm in diameter. The author (Wang, 2016) as a heat source in his experiment simulates the heat that should be generated by an engine with a low-pressure steam source (steam supply). The steam is transferred via a multi-pass heat exchanger to the cooling system, where the heated refrigerant then circulates through the convection automobile cooling system. The coolant flow circuit consists of a low pressure heat exchanger, an engine cooling jacket, a bypass valve, a variable speed coolant pump and a fan cooler. Safety devices such as a pressure regulator, a pressure gauge and a safety valve were inserted in the steam system. The steam flow was constant. Just as (Wang, 2016) secured the assembly against a sudden increase in pressure with safety valves, we also had to equip the heater connected to the cooling circuit with a vent pipe. In the event of a pressure increase, the refrigerant would circulate through the vent line back into the expansion vessel.

The size of the test circuit itself is an important factor for quality research. During the experimental work, it is important to work in a dry environment, where the heat losses to the environment are smaller and it is also necessary to ensure proper insulation of the test circuit (use of insulating material on the heater and fluid line of the test circuit) (Singh et al. 2017). The authors (Cuevas et al. 2011) heated a mixture of ethylene glycol and water in a ratio of 60:40 to an operating temperature of 90 °C. The test set-up consists of 3 circuits: primary, secondary and air, the primary and secondary circuits being used to adjust the flow and temperature of the glycol / water mixture. On the primary circuit there are two electric boilers for heating the cooling medium. The heat flow is transferred via a plate heat exchanger to the secondary circuit, where the tested heat exchanger is located. The temperature of glycol and water at the inlet to the cooler is regulated by changing the boiler output. In the authors' test set (Yadav & Singh 2011) there is a tank with a heating element (spiral), which acts as a heat source, which should act just like an engine in a car. A tin barrel with a volume of 40 l is used as a tank and the water was heated to a temperature of 65 – 75 °C. During testing, the maximum temperature at the inlet to the cooler was found to be 80 °C, while in fact the temperature of the coolant at the inlet to the cooler is much higher than in the experiment. At the beginning of their experiment, the authors (Hoseini et al. 2010) filled a reservoir with a heating coil with 8 liters of test liquid out of a total reservoir volume of 30 l (height 350 mm, diameter 300 mm - test liquid was filled to approximately 25% of the reservoir volume). The heating of the liquid and the maintenance of the temperature in the range of 40 to 80 °C was provided by a copper electric heater (spiral) with a regulator. The connection of the container with the components was realized by means of insulated pipes with a diameter of 19 mm. The tank with the spiral was, as in our case, equipped with a drain valve in the lower part, which will ensure complete draining of the liquid from the circuit in case of exchange for another type and thus to avoid undesired mixing of 2 types of liquids in the circuit. The authors (Peyghambarzadeh et al. 2013) performed heating of the coolant using two electric heaters with power regulation (6000 W) to change the temperature between 50 and 80 °C. They had 4 Pt-100 sensors installed on the flow pipe to record the inlet and outlet temperatures of the radiator fluids, the inlet air temperature and the last one was used in the tank to turn on / off the heaters (spirals).

The authors (Heris et al. 2014) used an experimental set-up in their research, which consisted of a liquid reservoir, a centrifugal pump, heating coils, a flow meter, a forced draft fan, an automobile radiator and a connecting pipe. They solved the problem of heating the liquid by using 6 cells with an output of 18,000 W with a regulator to maintain the temperature between 30 and 60 °C. The tank itself had a volume of 22 l and was filled with refrigerant. The total volume of the circuit was 25 l. Three-layer insulated pipes with a diameter of 19 mm were used as connecting pipes. The authors (Goudarzi & Jamali 2017) used a tank with a capacity of 18 l of coolant. There were 6 electric cells in the tank to increase the temperature of the liquid, similarly to the operation of the engine, the temperature was gradually rising to a value of approximately 80 °C. The experiment performed (Vasudevan Nambeesan et al. 2015) was performed at a constant flow rate and coolant inlet temperatures ranging from 40 to 70 °C. The set-up is a closed system and the coolant line consists of a reservoir, an electric heater, a pump and a radiator. The components are connected by means of pipes with a diameter of 25.4 mm. The liquid tank has a volume

of 90l. The coolant is heated in the tank by means of two electric spirals with a power of 1000 W. The authors (Ali et al. 2015) used a heater (Omega-CH-OTS-604/240 V, 6000 W) with a built-in temperature controller with an accuracy of ± 1 ℃ immersed in a liquid tank in the test set. The required radiator inlet temperature (45 ℃, 50 ℃ and 55 ℃) is set using the heater temperature controller.

In our article, we focused on the research of car radiators, the question arises how to generate this heat, as the combustion process does not take place and it is necessary to fully replace this heat and maintain it in the long term. The heat must be generated so that the thermostat can be opened and at the same time so that the thermal changes of the flowing refrigerant through the radiator can be monitored. Until the temperature reaches the value at which the thermostatic valve opens, the fluid flows through only a small motor circuit. After heating the liquid to the operating temperature (80 - 90 ℃), the thermostat starts to open and the liquid thus enters the large cooling circuit. It is also necessary to adapt this body to the real cooling circuit of the car so that the basic parameters of the cooling circuit do not change, which could further negatively affect the measurement processes.

As the size of the test circuit is an important factor, we focused on the development of a compact heating body. As mentioned above, the authors in their research heated a large amount of coolant at the same time, which resulted in a significant increase in the volume of coolant compared to the real engine cooling circuit in a car. Heating a higher volume of refrigerant can lead to measurement inaccuracies and at the same time leads to an increase in the energy consumption required to heat the coolant (stronger heating coil, longer heating time, etc.). The heater made by us has a small volume of coolant (1.9l) which leads to a reduction in energy consumption. Thanks to the smaller volume of the heating element, it is sufficient to use a heating spiral with a lower power (in our case 1500 W) as we do not heat a large volume of coolant at once, but gradually during the circulation of coolant through the circuit. The amount of coolant flowing through the heater corresponds to the volume of coolant flowing through the heating system in the car and thus there is no increase in the volume of coolant in the experimental setup compared to the real engine cooling circuit. This paper will be further devoted to the development of the heating element up to the very design of a new design solution.

MATERIAL AND METHODS

The engine cooling circuit is designed and constructed according to the real circuit in the car, but adapted to the laboratory environment and conditions. The principle of operation of the experimental set-up is shown in Fig. 1. The volume of refrigerant in the circuit is approximately 6 liters. The heating element (9) with the heating coil (12) was inserted behind the thermostatic valve (5) and in front of the water pump (13) by means of original connecting hoses, thus replacing the heating unit of the car.

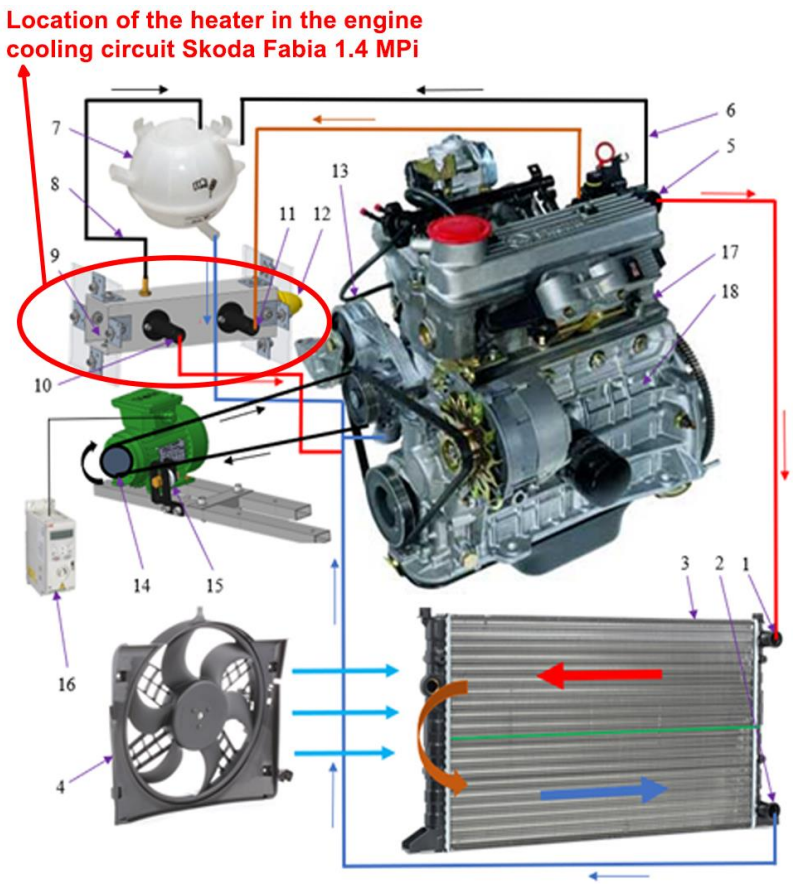

Fig. 1 The scheme of experimental assembly
1 – radiator inlet pipe, radiator outlet pipe, 3 – engine radiator, 4 – fan, 5 – thermostat, 6 – coolant return line, 7 – expansion tank, 8 – vent pipe, 9 – heater, 10 – coolant outlet, 11 – coolant inlet, 12 – heating spiral, 13 – water pump, 14 – electric motor, 15 – tensioning mechanism, 16 – frequency converter, 17 – engine head, 18 – engine block
Obr. 1 Schéma experimentálnej zostavy
1 – vstupné potrubie chladiča, 2 – výstupné potrubie chladiča, 3 – chladič motora, 4 – ventilátor, 5 – termostat, 6 – spätné potrubie chladiacej kvapaliny, 7 – vyrovnávacia nádobka, 8 – odvzdušňovacie potrubie, 9 – ohrevné teleso, 10 – výstupný nátrubok chladiacej kvapaliny, 11 – vstupný nátrubok chladiacej kvapaliny, 12 – ohrevná špirála, 13 – vodné čerpadlo, 14 – elektromotor, 15 – napínací mechanizmus, 16 – frekvenčný menič, 17 – hlava motora, 18 – blok motora

The cooling system is flooded with coolant through the expansion vessel (7). By starting the electric motor (14) using the frequency converter (16), start the water pump (13). The electric motor is connected to the water pump by a V-belt, which is tensioned by a mechanism (15). The experimental cooling system assembly has two cooling circuits (small and large). the cooling medium flows in a small cooling circuit at a temperature of up to 80 °C. It consists of a water pump (13) which drives the coolant through the cylinder

block (18), the cylinder head (17) and subsequently into the thermostat body (5). From there, the coolant is driven to the inlet of the heater (11). In the heating body (9), the coolant is heated by a heating coil (12), and the heated flows to the outlet nozzle (10). In the case of aeration or flooding of the heating element (9), a return pipe (8) is led from its upper part to the expansion vessel (7). The outlet nozzle of the heating element is connected by a pipe to a water pump. The coolant flows in a small circuit until the temperature rises above 80 °C. Subsequently, the thermostatic valve housed in the thermostat body (5) starts to open and the hot refrigerant flows to the inlet of the radiator (1). In the event that the hot liquid cannot flow under pressure through the cooler (3), a part of it flows through the return pipe (6) into the expansion vessel. The engine cooler (3) has the flow of heated flow medium divided into two parts and flows in the sense of the arrows shown in Fig. 1. Through the radiator outlet pipe (2), the cooled medium flows back to the water pump and from there back to a small circuit until the coolant temperature drops below 80 °C. If the coolant cannot be cooled by the engine radiator itself (3), the fan (4) is activated, which more intensively removes heat from the pipes and fins of the radiator.

The experimental set-up contains sensors for measuring the coolant temperature, namely NTC thermistors ZA 9040-FS (Negative Temperature Coefficient), whose electrical resistance is temperature dependent (Koleda et al. 2016). Their measuring range is -50 ℃ to 125 ℃, accuracy ± 0.01 ℃. Flow temperature sensors are located in the radiator inlet pipe (1), in the radiator outlet pipe Fig. 2a, in the thermostat housing Fig. 2b and in the heating body Fig. 2c.. The measured coolant temperatures are recorded on an ALMEMO 2590-4S value recorder.

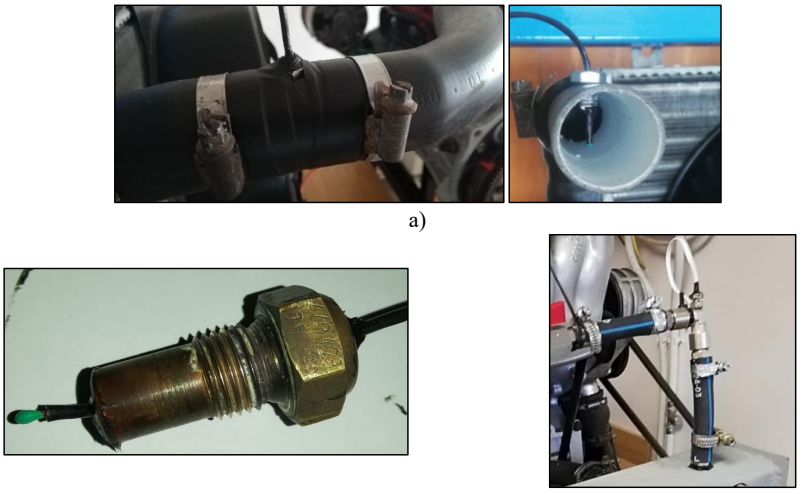

a) b) c)

Fig. 2 Placement of NTC resistance sensors in the experimental set up
a) placement in the cooling inlet and outlet pipes, b) placement in the thermostat housing, c) placement in the heater
Obr. 2 Umiestnenie odporových snímačov NTC v experimentálnej zostave
a) umiestnenie vo vstupnom a výstupnom potrubí chladiča, b) umiestnenie v obale termostatu, c) umiestnenie v ohrevnom telese

HEATING ELEMENT DESIGN

The design of the heater underwent gradual, based on test measurements, design changes and optimization (variants 1 to 3) to achieve real operating parameters of flow and heating time of coolants, and their smoother flow through the heater.

VARIANT 1

The first design and construction of the heater is shown in Fig. 3. The heater consisted of an expansion tank for coolant from a Skoda Favorit / Felicia vehicle. It was necessary to make a hole in the upper part of the tank for the inlet pipe connection. The hole was created with the help of a cut heating nozzle from a Skoda Fabia 1.4. Coolant entered the expansion tank through the inlet pipe from the outlet of the thermostat housing. The outlet of the expansion tank was connected to a pipe below the water pump, from where the heated liquid was pumped again by the water pump. The liquid return line in the upper part of the tank was connected to the expansion tank of the engine and also served as a vent pipe.

Fig. 3 Heater with a spiral of 500W
Obr. 3 Ohrevné teleso so špirálou o výkone 500W

In this case, a 500 W heating coil was to be used to heat the cooling medium. The expansion vessel was modified so that a heating coil could be fitted into it. Another problem encountered in this embodiment was the sealing around the spiral. This was solved by using engine sealant, up to a temperature of 180 °C.

VARIANT 2

Another version of the heating element differs structurally from variant 1, but the principle of heating the coolant is the same. A heating spiral with three branches, but with a power of 1500 W, was used for heating. The power of the heating coil had to be regulated, therefore a potentiometric power regulator was constructed (Fig. 8). Prior to the actual construction, a 3D model of the heating element was created in the Creo Parametric 7.0.1.0 program. The principle of operation of the heating element and its components are shown in Fig. 4.

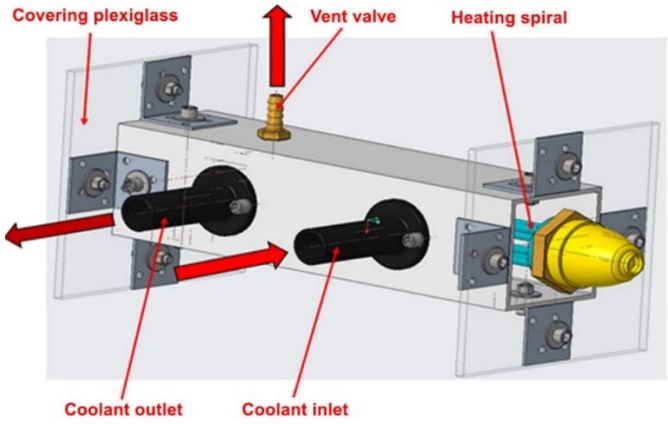

Fig. 4 Principle of operation and main parts of the heater
Obr. 4 Princíp činnosti a hlavné časti ohrevného telesa – variant 2

As can be seen in Fig. 4, the supporting element of the whole heating element assembly is an aluminum profile with dimensions of 80 × 80 × 300 mm. This profile also serves as a vessel into which a heating coil is inserted from the side through the plexiglass. During the operation of the heating element, the aluminum profile is encapsulated with a cooling liquid, which is heated by a heating coil. Nozzles are used for the inlet and outlet of the coolant, on which rubber water hoses are mounted. A nozzle is inserted into the upper part of the profile, which serves as a vent valve. The vent valve located in the upper part of the heating element serves for continuous venting of the entire small circuit. Air bubbles or excess coolant are returned to the expansion tank. In the absence of this valve, an overpressure could be created throughout the system and consequent damage to the heater, even though a thermostat has been used which has an opening outside the valve itself to release pressure or a small amount of liquid. The coolant flowing through the orifice enters a large cooling circuit to the radiator. The profile is closed by two pieces of plexiglass, one plexiglass is complete and the other has a hole with a diameter of ø 47 mm for fixing the heating coil. The heating coil is attached to the plexiglass with a brass nut Fig. 5.

Fig. 5 Connecting the heating element to the experimental set up
Obr. 5 Pripojenie ohrevného telesa k experimentálnej zostave

When the heater was in operation, i.e. the liquid heated by the spiral flowed through it, thermal imaging images of the heater and its components were recorded by a Flir i7 thermal imaging camera. For correct function and correct measurement result, it is necessary to set the emissivity of the surface of the material to be scanned. The emissivity for aluminum is 0.25 and for rubber is 0.94. By measuring the temperature with an infrared thermometer or a thermal imager, the amount of energy that radiates / reflects the measured object to the instrument itself is measured (Wang et al. 2015). The temperatures on the inlet and outlet nozzles differed. The temperature difference was approximately 3 °C, the outlet nozzle always having a higher temperature Fig. 6. The reason for the lower temperature at the inlet is that the coolant has transferred some of the heat through the pipe walls and the motor in the cooling circuit.

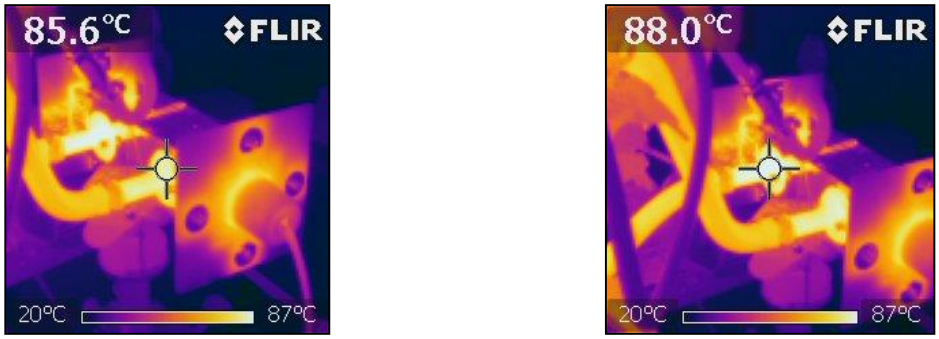

a) b)

Fig. 6 Thermal images of a heater
a) inlet pipe temperature sensing, b) outlet pipe temperature sensing
Obr. 6 Termovízne obrazy ohrevného telesa
a) snímanie teploty vstupného nátrubku, b) snímanie teploty výstupného nátrubku

VARIANT 3

The third variant of the heating element differs slightly in construction from variant 2 (Fig. 7). In this case, the heating element is profiled steel with a thickness of 3 mm and the joints were not sealed with sealant, but with welds. As a result, the heating element forms one unit, which minimizes the possibility of coolant leakage even at high temperatures. Variant 3 is designed to handle long-term loads of high temperatures and pressures. The principle of heating the coolant remained practically the same. The same type of heating coil as in variant 2 was used. Of the three branches of the heating coil, only 2 branches were connected, which provided us with sufficient power for our experiment (1000 W).

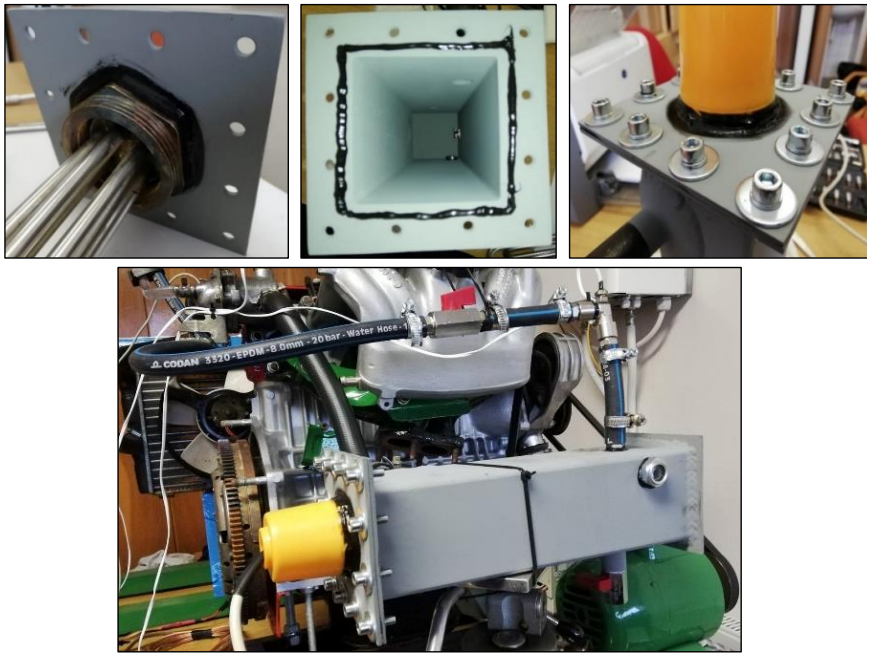

Fig. 7 Construction and connection of the heater to the experimental set up
Obr. 7 Konštrukcia a napojenie ohrevného telesa k experimentálnej zostave

HEATING SPIRAL

Power supply and temperature regulation of the heating coil is solved by means of a triac regulator. Via resistor R2, trimmer Trim and potentiometer Pot Fig. 8 is a charged capacitor C2. As soon as the voltage at its terminals reaches the breakdown voltage of the diac, which is about 32 V for the DB3, the diac reaches a conductive state and this voltage is connected to the control electrode (G) of the triac. This voltage pulse opens the triac. The voltage across the capacitor drops, but the open triac remains open until the supply voltage drops below the holding voltage level. The higher the resistance of the cascade R2, trimmer, potentiometer, the longer it will take to charge the capacitor, so the triac will be open for a shorter time, the smaller the mean value of the output voltage. The trimmer is used for coarse adjustment of the resistance, potentiometer for fine adjustment and for the required voltage regulation.

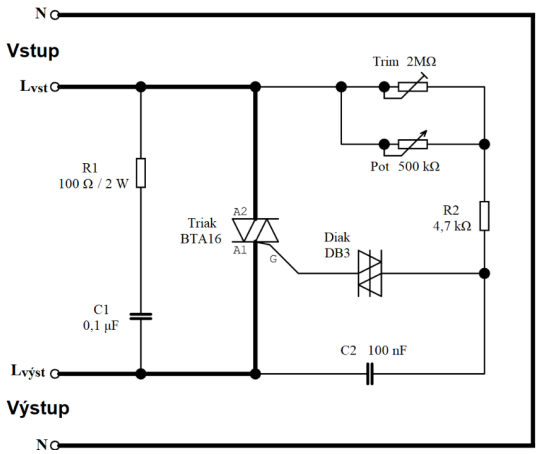

Fig. 8 Wiring diagram of the triac controller
Obr. 8 Schéma zapojenia triakového regulátora

RESULTS AND DISCUSSION

By performing individual experiments and measurements, we gradually found the shortcomings of heating elements for possible modifications and optimization (variants 1 to 3), which were used in the experimental set of the cooling circuit of the Skoda Fabia 1.4 MPI engine.

Using the first variant, we found that by gradually heating the coolant, its temperature stabilizes at a value of about 60 ℃. Since we needed to reach a higher temperature for about 6l of coolant, this method was not sufficient. Another problem was the heat leakage through the aluminum components of the engine, which had to be gradually heated to a temperature of about 80 ° C, but this failed. The heated liquid from the coil, which circulated in a small circuit, gradually cooled as heat was removed to the walls delimiting the cooling channels. The desired temperature to be achieved was about 90 ° C. At higher spiral power, such a design would work.

In the second variant of the heating element, during the long-term heating of the liquid to approximately 90 ℃, the cover plexiglass cracked and bulged, which resulted in a broken seal (between the Al profile and the cover plexiglass) and subsequent undesired leakage of coolant in small amounts. A great advantage of the cover plexiglass was the easy determination of the coolant level in the body itself. If the liquid level was below the upper edge, we knew that there was an air bubble in the heater, which had to be removed by means of a ball valve and a vent line. Another disadvantage of variant 2 was the material of the body itself - an aluminum profile through which the walls quickly escaped heat from the heating body to the surrounding environment. We also wanted to know the value of the coolant temperature around the coil, but in this design the temperature sensor was absent at this point.

In the case of the third, most satisfactory and currently used variant of the heating element, none of the above-mentioned shortcomings appears and its operation is problem-free even under long-term loading. However, if we want to get as close as possible to real

conditions, and thus achieve the least distorted measured values, it is necessary to oversize this body for a smaller volume of coolant. The required volume of the cooling circuit is set by the manufacturer at 5.6 liters for the given engine. Based on these findings, we designed a new design of the heating element, in which the above-mentioned problems were eliminated (Fig. 9b). The designed square radiator with a cross-section of 80 × 80 × 300 mm with a volume of 1.9 l was replaced by a radiator with a circular cross-section ø 80 × 300 mm with a volume of 1.5 l to reduce the volume of coolant in the experimental set and its shorter heating at the manufacturer's 5.6 l. The proposed circular heater, compared to a square heater, is shown in the form of 3D models created in Creo Parametric 7.0.1.0 in Fig. 9.

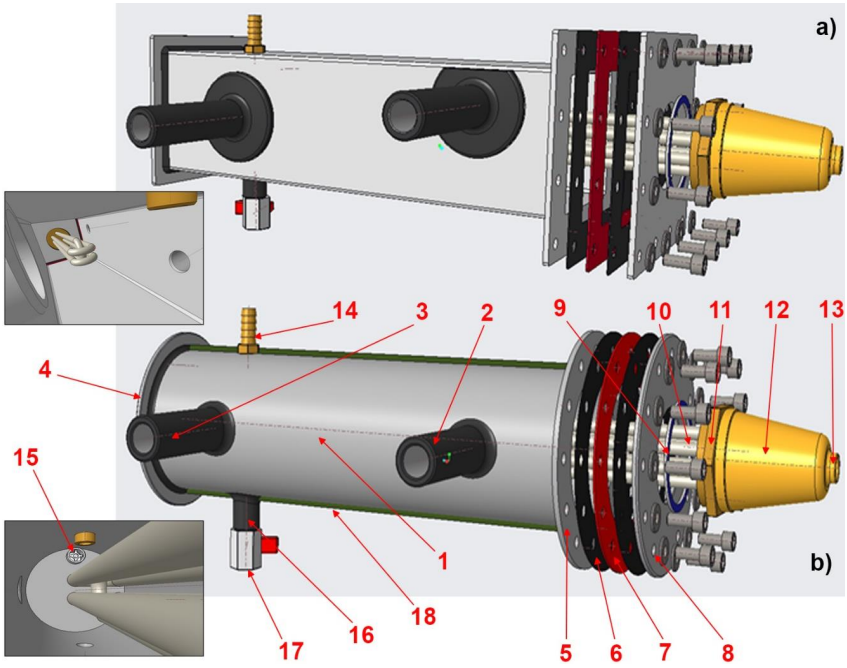

Fig. 9 3D models of heaters and their individual parts
a) currently used heater, b) newly designed heater
1 – core of the heater, 2 – coolant inlet, 3 – coolant outlet, 4 – rear flange of the heater, 5 – front flange of the heater, 6 – silicone sealant, 7 – sealing paper, 8 – closing lid with spiral hole, 9 – fiber seal, 10 – heating spiral, 11 – spiral base plate with power pins, 12 – spiral power cover, 13 – spiral power input, 14 – socket for vent pipe (temperature sensor inlet), 15 – watermark, 16 – welding tube, 17 – drain ball valve, 18 - isolation

Obr. 9 3D modely ohrevných telies a ich jednotlivých častí
a) aktuálne používané ohrevné teleso, b) novo navrhnuté ohrevné teleso 1 – jadro ohrevného telesa, 2 – vstupný nátrubok chladiacej kvapaliny, 3 – výstupný nátrubok chladiacej kvapaliny, 4 – zadná príruba ohrevného telesa, 5 – predná príruba ohrevného telesa, 6 – silikónový tmel, 7 – tesniaci papier, 8 – záverné veko s otvorom pre špirálu, 9 – fibrové tesnenie, 10 – ohrevná špirála, 11 – základová doska špirály s kolíkmi pre napájanie, 12 – kryt napájania špirály, 13 – vstup napájania špirály, 14 – nátrubok pre odvzdušňovacie potrubie (vstup snímaču teploty), 15 – vodoznak, 16 – navarovacia rúrka, 17 – vypúšťací guľový ventil, 18 – izolácia

CONCLUSION

The issue of heat transfer is currently a main topic in terms of energy savings, economics of operation, eventualy effective cooling. In order to ensure a more efficient heat exchange process, it is necessary to examine the physical and geometrical parameters of heat exchange systems of heat exchangers. Due to the development of automobile engines and the increase in their performance parameters, it is necessary to continuously adjust the radiators, because about a third (and more) of the thermal energy produced by internal combustion engines passes as waste heat through the cooling system. Research and development in this area is carried out in order to reduce fuel consumption and comply with current emission limits.

The article deals with the design of a suitable heating element for the research of car radiators in the laboratory. Since the engine of the proposed experimental set-up for the research of compact heat exchangers, in our case coolers, does not produce heat by the combustion process, the coolant heating system plays an important role. However, it is necessary to oversize and design this system so that it works as efficiently as possible and does not cause measurement inaccuracies (heating a large amount of liquid, low heating coil power, leaks, etc.).

Gradually, designs and constructions of heating elements were realized, which underwent changes and optimization (variants 1 to 3) in order to achieve real operating parameters of flow and heating time of coolants. The third variant of the heating element best suits the experimental conditions in the laboratory even under long-term loading (flow, temperature, pressure). However, when using a square cross-section of the heating element, the volume of the cooling circuit reaches approximately 6 l, therefore its shape has been adjusted to a circular cross-section of ø 80 mm to achieve a volume of cooling circuit specified by the manufacturer of 5.6 l. This proposal will reduce the volume of coolant and the experimental set will be equal to the real cooling circuit of the car, which will also obtain more accurate values from subsequent measurements of the thermal parameters of various car radiators.

ACKNOWLEDGMENT

The contribution was created with the financial support of the Ministry of Education, Science, Research and Sports of the Slovak Republic within the project VEGA 1/0086/18 Research of temperature fields in the system of shaped heat exchange surface within the project IPA 2/2021 Modification of cooling method of compact heat exchanger in engine cooling circuit car.

REFERENCES

ALI, H. M., ALI, H., LIAQUAT, H., MAQSOOD, H. T. B., NADIR, M. A., 2015. Experimental investigation of convective heat transfer augmentation for car radiator using ZnO-water nanofluids. In Energy, 2015, Elsevier, vol. 84, pages 317-324. DOI: 10.1016/j.energy.2015.02.103.

CUEVAS, C., MAKAIRE, D., DARDENNE, L. NGENDAKUMANA, P. 2011. Thermo-hydraulic characterization of a louvered fin and flat tube heat exchanger. In Experimental Thermal and Fluid Science. ISSN 0894-1777, 2011, vol. 35, p. 154-164.

GOUDARZI, K., JAMALI, H., Heat transfer enhancement of Al_2O_3-EG nanofluid a car radiator with wire coil inserts. In Applied Thermal Engineering, 2017, vol. 118, pages. 510-517, DOI: 10.1016/j.applthermaleng.2017.03.016.

HERIS, S. Z., SHOKRGOZAR, M., POORPHARHANG, S., SHANBEDI, M., NOIE, S. H., 2014. Experimental Study of Heat Transfer of a Car Radiator with CuO/Ethylene Glycol-Water as a Coolant. In Journal of Dispersion Science and Technology, 2014, vol. 35, Issue 5, pages. 677-684, ISSN: 0193-2691.

HOSEINI, S. M., SEIFI JAMNANI, M., PEYGHAMBARZADEH, S. M., HASHEMABADI, S. H., 2010. Experimental Study of Water and Ethylene Glycol Mixture Heat Transfer in the Automobile Radiator. In Iranian National Chemical Engineering Congress, 2010, vol. 10.

HUSSEIN, A. M., BAKAR, R. A., KADIRGARGAMA, K., SHARMA, K. V., 2014. Heat transfer enhacement using nanofluids in an automotive cooling system. In International Communications in Heat and Mass Transfer, 2014, vol. 53, pp. 195-202. DOI: 10.1016/j.icheatmasstransfer.2014.01.003.

KOLEDA, P., KOLEDA, P., GRÚBEL, S. 2016. Analysis of temperatures in the mould area during the process of engine cylinder heads casting. Acta Facultatis Technicae, XXI, 2016 (1), pp. 31-40. ISSN 1336-4472.

PEYGHAMBARZADEH, S. M., HASHEMABADI, S. H., NARAKI, M., VERMAHMOUDI, Y., 2013. Experimental study of overall heat transfer coefficient in the application of dilute nanofluids in the car radiator. In Applied Thermal Engineering, 2013, vol. 52, Issue 1, Pages 8-16, DOI: 10.1016/j.applthermaleng.2012.11.013.

SINGH, S., KUMAR, A., KHAN, F., 2017. Experimental study for heat transfer enhacement of car radiator using twisted inserts with coolants. In International Journal of Interdisciplinary Research, 2017, vol. 3, Issue 1, ISSN 2455-1600.

VASUDEVAN NAMBESAN, K. P., PARTHIBAN, R., RAM KUMAR, K., ATHUL, U. R., VIVEK, M., THIRUMALINI, S., 2015. Experimental study of heat transfer enhancement in automobile radiator using Al_2O_3/water-ethylene glycol nanofluid coolants. In International Journal of Automotive and Mechanical Engineering (IJAME), 2015, vol. 12, pp. 2857-2865, ISSN: 2229-8649.

WANG H., CAI Y., WANG W., A 2017: dynamic thermal – mechanical model of the spindle – bearing system, Key Laboratory of Vehicle Advanced Manufacturing, Measuring and Control Technology, Ministry of Education, Beijing, 100044, China. ISSN 2191-9151.

WANG, T. T., 2016. Investigation of Advanced Engine Cooling Systems – Optimalization and Nonlinear Control. All Dissertations. 1647. Dostupné na: https://tigerprints.clemson.edu/cgi/viewcontent.cgi?article=2648&context=all_dissertations

YADAV, J. P., SINGH, B. R. 2011. Study on performance evaluation of automotive radiator. In Samriddhi: A Journal of Physical Sciences, Engineering and Technology, 2011, vol. 2, Issue 2, pp. 47-56, ISSN 2229-7111.

Corresponding author:
Ing. Marek Lipnický, tel.: +421455206 053, e-mail: xlipnicky@tuzvo.sk

THE USE OF SMART SYSTEMS FOR THE PREPARATION OF A TOTAL MIXED RATION FOR DAIRY COWS

VYUŽITIE INTELIGENTNÝCH SYSTÉMOV PRI PRÍPRAVE ZMIEŠANEJ KŔMNEJ DÁVKY PRE DOJNICE

Gabriel Lüttmerding, Roman Gálik, Štefan Boďo

Department of Building Equipment and Technology Safety, Faculty of Engineering, Slovak University of Agriculture in Nitra, Tr. A. Hlinku 2, 949 76, Nitra, Slovakia, xluttmerding@uniag.sk

ABSTRACT: The total mixed ration represents an optimal composition of the very most needed raw materials in order to create the most optimal inputs the livestock needs, so farmer receives the highest possible quality outputs, such as high quality milk & meat, but most importantly the animal welfare must not be forgotten. Precision agriculture is seen as the future of agriculture and the data transfer is a crucial parameter for the digitalization in these days, or in the very near future. Dairy farming with the use of the data transfer between the feed mixer wagon and the farmer is the perfect combination to ease the work labour as well as to increase the level of the quality of work, and lastly but not least – the health of the livestock.

Key words: digitalization; precision agriculture; total mixed ration; dairy cattle; mixer feed wagon

ABSTRAKT: Zmiešaná kŕmna dávka predstavuje optimálne zloženie tých najpotrebnejších surovín pre vytvorenie optimálnych vstupov, ktoré hospodárske zvieratá potrebujú, aby farmár dostal tie najkvalitnejšie výstupy, či už ide o kvalitné mlieko & mäso, ale najmä o pohodu zvierat, na ktorú sa nemá zabúdať. Precízne poľnohospodárstvo predstavuje budúcnosť poľnohospodárstva a data transfer je kritický parameter, bez ktorého sa digitalizácia v poľnohospodárstve či už v dnešnej dobe, alebo v blízkej budúcnosti, nezaobíde. Chov dojníc, spolu s využitím data transferu medzi miešacím kŕmnym vozom a farmárom, predstavuje perfektnú kombináciu, ako si uľahčiť prácu na farme, ako aj zvýšiť úroveň kvality práce a netreba zabúdať predovšetkým na zdravie hospodárskych zvierat.

Kľúčové slová: digitalizácia; precízne poľnohospodárstvo, zmiešaná kŕmna dávka; dojnice; miešací kŕmny voz

INTRODUCTION

Feeding operations in dairy cow farms are of strategic importance for the economy of the farm. Aside from being strictly related to the productivity of the cows, feeding represents one of the greater costs for farms, considering that more than 25 % of labour time is

dedicated to this operation (Pezzuolo et al., 2015). Dairy farmers are increasingly evolving toward automation of their farms (Boscaro et al., 2015; Marinello et al., 2015). Automatic concentrate dispensers and automatic milking systems (AMS) have been utilized for years, and several manufacturers have introduced automatic feeding systems (AFS) during the past decade (Belle et al., 2012; Unal & Kuraloglu, 2015). The main advantage of the AFS is the possibility to supply a total mixed ration (TMR) with a high frequency and a low labour requirement, whilst farms which feed with conventional feeding systems (CFS) commonly supply TMR only once or twice a day and require more labour with a rigid work schedule. (DeVries et al., 2005). According to the well known literature, a total mixed ration (TMR) is a feeding system, used to provide consistent feed to animals and to stabilize rumen conditions as desired. Feeding activities have an important place in terms of animal health, performance, milk yield or meat production. Because of these and many other reasons to implement the TMR, these mixtures should be regular and very stable. The very each mouthful of the mixture consumed by an animal, must be homogenous and balanced, otherwide the animal can be negatively affected. The ration created by a farmer and the ration delivered to the cow are sometimes very different, despite a lot of time and a lot of effort is already made (Sova et al., 2014). Many strategies can be used in TMR systems. These mixtures can be formulated for fresh cows, early lactation cows, mid-lactation as well as late-lactation, or close-up dry cows. Cows can be placed in groups created, which are based on actual or fat-corrected milk, days in milk, reproductive status, age, nutrient requirements and health. There are many reasons to introduce different strategies for using TMR and there must be a decision of a farm manager, based on many aspects of the operations, research and personal preferences (Heinrichs & Kmicikewycz, 2016). The aim of this paper is to point out how crucial the data transfer is for the farmer, to see the weight deviations of the set and the actual weight of the components, put into the TMRs. The data were obtained through a vertical feed mixer wagon and the results are put into the tables and graphs, which do show how precise the loading of the components really is. In our work we established a hypothesis that the difference between the set and the actual loaded weight of the feed ration put into the mixer feed wagon, will not be greater than ± 5 %.

MATERIAL AND METHODS

Measurements for this article were made on a selected agricultural holding, using a Trioliet Solomix 2 1200 ZK (1 wheel axle) mixer feed wagon, shown on the Figure 1. The data of the selected feed rations were transfered from the mixer feed wagon to the usb stick. These data were exported into the PC and processed in the chosen software. We chose 3 groups of dairy cows with the highest milk yield. We could choose from many parametres, although we focused mainly on the set weight and the actual loaded weight. The weight differences were calculated from the chosen data. An acceptable permissible limit of ± 5 % was chosen by us. We chose data from the 10 days for the each group of cows. All the results were processed in tables and figures, which do show the difference between the set weight and the actual loaded weight of the feed ration components, exceeding the chosen maximal permissible limit.

Characteristics of the Trioliet Solomix 2 1200 ZK (1 wheel axle) mixer feed wagon

Fig. 1 Trioliet Solomix 2 1200 ZK (1 wheel axle)
Obr. 1 Trioliet Solomix 1200 ZK (1 náprava)

Technical data of the Solomix 2 1200 ZK are shown in the Table 1.

Table 1. Basic technical data of Trioliet Solomix 2 1200 ZK (1 wheel axle)
Tabuľka 1. Základné technické údaje Trioliet Solomix 2 1200 ZK (1 náprava)

Volume [1] [m³]	12
Length [2] [m]	6.05
Width [3] [m]	2.24
Height [4] [m]	2.50
External width on wheels [5] [m]	1.71
Height when unloading [6] [m]	0.82
Height when unloading with an extension [7] (extra) [m]	0.98 – 1.31
Unloading width [8] [m]	0.92
Payload [9] [kg]	4 500
Number of knives/counter-blades [10] [pcs]	4/2
Tires [11] [class]	2x 400/45 L17.5
Tractor (min. HP) [12] [HP]	82

[1] Objem, [2] DÍžka, [3] Šírka, [4] Výška, [5] Vonkajšia šírka na kolesách, [6] Výška pri vykladaní, [7] Výška pri vykladaní s nástavcom (extra výbava), [8] Šírka pri vykladaní, [9] Užitočná hmotnosť, [10] Počet nožov/protiostria, [11] Pneumatiky, [12] Traktor (min. HP)

The characteristics of the selected groups of dairy cows

As shown in the Table 2, there are the labels and the characteristics of the selected groups of the dairy cows. In order to comply with the required scope of this contribution, we did select only three groups. They do differ mainly in color or another feature. According to the instructions and privacy of the selected agricultural holding, we were provided only with basic information.

Table 2. The characteristics of the selected groups of the dairy cows
Tabuľka 2. Charakteristika vybraných skupín dojníc

Label [1)]	Description [2)]
A	The top group, milk yield over 35 liters
B	Subgroup, different number of cows, different breed color, milk yield up to 35 liters
C	Subgroup, different number of cows, different breed color, milk yield up to 35 liters

[1)] Označenie, [2)] Opis

The characteristics of the feed ration components

The chosen groups of animals were fed by the feed ration of the same structure, composed of four main components. The Table 3 shows the chosen components of the feed ration, and the numbers provided for the each component, which helped us to differ the data in our research.

Table 3. Charakteristics of components of selected groups of dairy cows
Tabuľka 3. Charakteristika komponentov kŕmnych dávok vybraných skupín dojníc

Number [1)]	Component [2)]
1	Core concentrate
2	Lantern haylage
3	Corn silage
4	Water

[1)] Číslo komponentu, [2)] Opis

Analysis methods and evaluation of results

As we mentioned before, the set weight and the actual loaded weight of the feed ration were used. Using the basic mathematical methods, we did calculate the total set weight and the total actual loaded weight of all the components of the feed ration (Eq. 1, Eq. 2):

$$w_{s_t} = w_{s_{c_1}} + w_{s_{c_2}} + w_{s_{c_3}} + w_{s_{c_4}} \quad (1)$$

$$w_{a_t} = w_{a_{c_1}} + w_{a_{c_2}} + w_{a_{c_3}} + w_{a_{c_4}} \quad (2)$$

where

w_{s_t} - total set weight [kg],
$w_{s_{c_1}}$ - set weight of the component 1 [kg],
$w_{s_{c_2}}$ - set weight of the component 2 [kg],
$w_{s_{c_3}}$ - set weight of the component 3 [kg],
$w_{s_{c_4}}$ - set weight of the component 4 [kg],

w_{a_t} - total actual weight [kg],
$w_{a_{c_1}}$ - set weight of the component 1 [kg],
$w_{a_{c_2}}$ - set weight of the component 2 [kg],
$w_{a_{c_3}}$ - set weight of the component 3 [kg],
$w_{a_{c_4}}$ - set weight of the component 4 [kg].

Subsequently, in order to find out the percentage deviations between the set and actual loaded weight in the group, we did use the following Equation 3:

$$w_d = \frac{w_{a_t} - w_{s_t}}{w_{a_t}} . 100 \quad (3)$$

where w_d – weight difference [%],

RESULTS AND DISCUSSION

Group A

From the calculations we made, we did find out in the group A there were no exceedings bigger than the permissible limit ± 5 % set by us. The minimum weight difference was + 0.03 %, the maximum weight difference did not exceed + 4.15 % and the average value was + 0.82 %. The Table 4 shows the weight differences between the set weight and the actual loaded weight during 10 days, as well as the minimum, maximal and average values.

Table 4. Differences of set weight and actual weight in the group A
Tabuľka 4. Rozdiely nastavenej a skutočne naloženej hmotnosti v skupine A

Day [1]	Day 1	Day 2	Day 3	Day 4	Day 5	Day 6	Day 7	Day 8	Day 9	Day 10
Weight difference [2] [%]	4.15	0.28	0.28	0.51	0.53	0.91	0.15	0.41	0.03	0.91
MIN [3] [%]	+ 0.03									
MAX [4] [%]	+ 4.15									
AVERAGE [5] [%]	+ 0.82									

[1] Deň merania, [2] Rozdiel hmotností, [3] Minimálna hodnota, [4] Maximálna hodnota, [5] Priemer hodnôt

On the Figure 2 are shown the weight differences during the 10 days in the group A with an indication of the maximal and minimal permissible limit set by us.

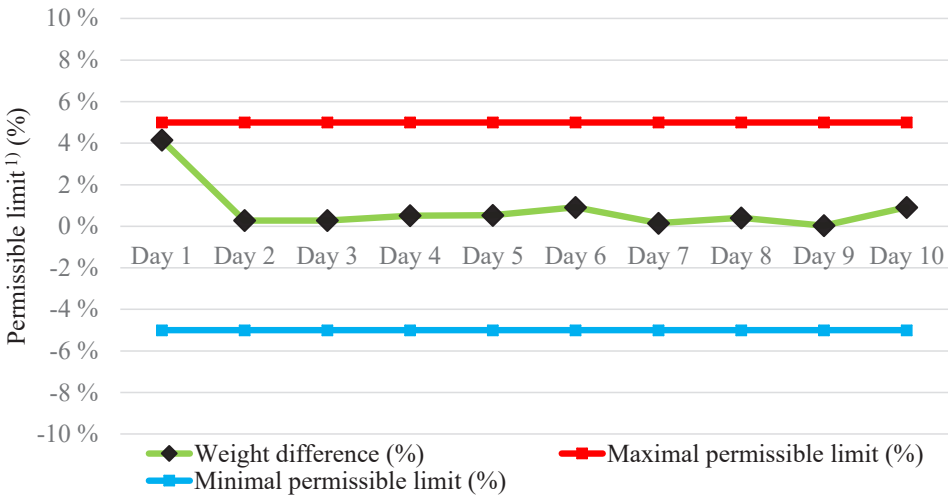

Fig. 2. Group A
Obr. 2. Skupina A
[1] Prípustná hranica

Group B

From the calculations we made, we did find out in the group B there were no exceedings bigger than the permissible limit ± 5 % set by us. The minimum weight difference was + 0.24 %, the maximum weight difference did not exceed + 1.40 % and the average value was + 0.63 %. The Table 5 shows the weight differences between the set weight and the actual loaded weight during 10 days, as well as the minimum, maximal and average values.

Table 5. Differences of set weight and actual weight in the group B
Tabuľka 5. Rozdiely nastavenej a skutočne naloženej hmotnosti v skupine B

Day of measurement [1]	Day 1	Day 2	Day 3	Day 4	Day 5	Day 6	Day 7	Day 8	Day 9	Day 10
Weight difference [2] [%]	1.4	0.59	0.41	0.24	0.33	0.33	0.81	0.49	0.47	1.25
MIN [3] [%]	+ 0.24									
MAX [4] [%]	+ 1.4									
AVERAGE [5] [%]	+ 0.63									

[1] Deň merania, [2] Rozdiel hmotností, [3] Minimálna hodnota, [4] Maximálna hodnota, [5] Priemer hodnôt

On the Figure 3 are shown the weight differences during the 10 days in the group B with an indication of the maximal and minimal permissible limit set by us.

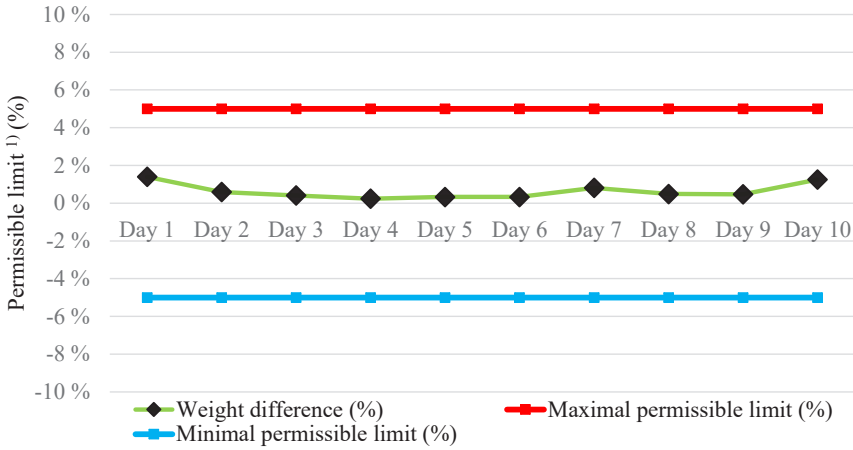

Fig. 3. Group B
Obr. 3. Skupina B
[1] Prípustná hranica

Group C

From the calculations we made, we did find out in the group C there were no exceedings bigger than the permissible limit ± 5 % set by us. The minimum weight difference was – 0.06 %, the maximum weight difference did not exceed + 2.37 %

and the average value was + 0.61 %. The Table 6 shows the weight differences between the set weight and the actual loaded weight during 10 days, as well as the minimum, maximal and average values.

Table 6. Differences of set weight and actual weight in the group C
Tabuľka 6. Rozdiely nastavenej a skutočne naloženej hmotnosti v skupine C

Day of measurement [1]	Day 1	Day 2	Day 3	Day 4	Day 5	Day 6	Day 7	Day 8	Day 9	Day 10
Weight difference [2] [%]	0.61	0.81	0.09	0.09	- 0.06	2.37	0.38	0.38	0.63	0.79
MIN [3] [%]	- 0.06									
MAX [4] [%]	+ 2.37									
AVERAGE [5] [%]	+ 0.61									

[1] Deň merania, [2] Rozdiel hmotností, [3] Minimálna hodnota, [4] Maximálna hodnota, [5] Priemer hodnôt

On the Figure 4 are shown the weight differences during the 10 days in the group C with an indication of the maximal and minimal permissible limit set by us.

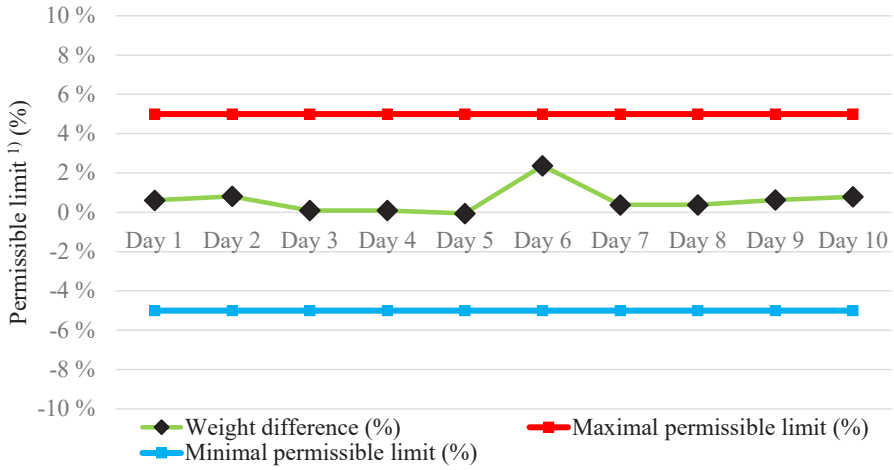

Fig. 4. Group C
Obr. 4. Skupina C
[1] Prípustná hranica

The results of our work shown we have not noticed a significant difference between the set and the actual weight of the individual components loaded into the hull of the mixer feed wagon. The mixer feed wagon we used has the vertical mixing augers and has no loader. We found the operator of the separate loading device was accurately guided by the information provided by the wagon›s weighing system and the deviations from the set value of the weight did not exceed ± 5 %. Kowalik et al., (2018) also achieved similar results, when the quality of the work of feed mixer wagons with both horizontal and vertical augers was compared. In their research they assessed the accuracy of loading the TMR compo-

nents. They did use three mixer feed wagons with the vertical augers, one mixer feed wagon with a horizontal crushing & mixing system and a self-loader, as well as one self-propelled mixer feed wagon with a vertical crushing & mixing system and a self-loading equipment. Whilst in our TMR we only had 4 components available, the cited author had 2 TMRs available, the first one with 7 components and the second one with up to 10 components. Sirakaya & Küçük (2019) also dealed with a similar topic, examining the deviations from the set weight of loading the TMR components into the mixer feed wagon. The authors tried to determine the value of the deviation according to the TMR preparation operators, then the type of the loader, the physical properties of the feed, the method of loading the feed, the type of feed ration and the type of component. A significant percentage differences were found between different operators. The devation range was between 5.48 % and 12.23 %. Work discipline and the ability to operate could be the reasons of this difference. This could be fixed by providing a quality staff training, subsequent remedies and the change of the work discipline.

CONCLUSION

We do can conclude the established hypothesis was confirmed. We did prove the weight differences of the feed ration did not exceed the set permissible limit ± 5 %. To be precise, in the first group the weight differences were in the range of ± 4,15 %, in the second group it was no more than ± 1,40 %, followed by the third group with the range of ± 2,37 %. These different range percentages could be caused by the dimension differences of the feed, as the core feed has smaller particles than the ones in the bulk feed. We can say the core feed was loaded more precisely than the bulk feed.

Although the mixer feed wagon we used the data from has no loader, and the loading is based on the manual external loading machine, we can say the feeding system works better than we expected. There are many types of these mixer feed wagons, whether it is a self-propelled one or the one with a built-in loader, but at the end of the day, it is the human & machine relationship, which really does matter. Thanks to the data transfer between the mixer feed wagon and the local network on the farm we had the data from, it is now easier than ever to use the numbers to create these inputs in a matter of minutes.

The machinery is getting better every single day and it will not stop innovating. As the mankind evolves, so does the machinery, whether is is the IT sector, which represents the data transfer or the mixer feed wagons in the agricultural sector. These very two sectors should work together and create a better and greener future for humanity and also, last but not least, for the dairy cows.

ACKNOWLEDGEMENT

This publication was supported by the Operational Programme Integrated Infrastructure within the project: Sustainable smart farming systems taking into account the future challenges 313011W112, cofinanced by the European Regional Development Fund.

LITERATURE

BELLE, Z., ANDRÉ G., POMPE, J.C.A.M., 2012. Effect of automatic feeding of total mixed rations on the diurnal visiting pattern of dairy cows to an automatic milking system. *Biosystems Engineering*, vol. 111, pp. 33-39, ISSN 1537-5110. **[**online**].** Available at: <https://www.sciencedirect.com/science/article/pii/S1537511011001802>.

BOSCARO, D., PEZZUOLO, A., GRIGOLATO, S., CAVALLI, R., MARINELLO, F., SARTORI L., 2015. Preliminary analysis on mowing and harvesting grass along riverbanks for the supply of anaerobic digestion plants in north-eastern Italy. *Journal of Agricultural Engineering*, vol. 46, pp. 100-104. 10.4081/jae.2015.465. **[**online**].** Available at: <https://www.researchgate.net/publication/282973813_Preliminary_analysis_on_mowing_and_harvesting_grass_along_riverbanks_for_the_supply_of_anaerobic_digestion_plants_in_North-Eastern_Italy>.

DeVRIES, T.J., von KEYSERLINGK, M.A.G., BEAUCHEMIN, K.A., 2005. Frequency of feed delivery affects the behavior of lactating dairy cows. *Journal of Dairy Science*, vol. 88, issue 10, pp. 3553-3562. ISSN 0022-0302. [online]. Available at: <https://www.sciencedirect.com/science/article/pii/S002203020573040X>.

GÁLIK et al., 2018. *Technika pre chov zvierat*. 2. vyd. Nitra: Slovenská poľnohospodárska univerzita v Nitre. ISBN 978-80-552-1906-6.

HEINRICHES, J., KMICIKEWYCZ, A., 2016. Total Mixed Rations for Dairy Cows. [online]. Available at: <https://extension.psu.edu/total-mixed-rations-for-dairy-cows>.

KOWALIK et al., 2018. A comparison of quality of work of the feed mixer wagons with vertical and horizontal mixing systems. 2018. [online]. Available at: <http://yadda.icm.edu.pl/baztech/element/bwmeta1.element.baztech-da120c0d-f6a6-4a9e-9bee-1cf6137a2e60>.

MARINELLO, F., PEZZUOLO, A., GASPARINI, F., ARVIDSSON, J., SARTORI, L., 2015. Application of the Kinect sensor for dynamic soil surface characterization. *Precision Agriculture*, vol. 5, pp. 1-12. 16. 10.1007/s11119-015-9398-5. [online]. Available at: <https://www.researchgate.net/publication/276458483_Application_of_the_Kinect_sensor_for_dynamic_soil_surface_characterization>.

PEZZUOLO, A., MAGRIN, L., COZZI, G., MARINELLO, F., SARTORI, L., 2015. Precision and efficiency of a mechanized delivery system of solid feeds for veal calves. pp. 465-472. [online]. Available at: <https://www.researchgate.net/publication/288269017_Precision_and_efficiency_of_a_mechanized_delivery_system_of_solid_feeds_for_veal_calves>.

SIRAKAYA, S., KÜÇÜK, O., 2019. Deviations of feedstuff loading in TMR preparation. [online]. Available at: <https://www.cabdirect.org/cabdirect/abstract/20193289080>.

SOLOMIX 2 - Mixer feeder wagons models 1000 - 3200. **[**online**].** Available at: <https://www.google.com/url?sa=t&rct=j&q=&esrc=s&source=web&cd=&cad=rja&uact=8&ved=2ahUKEwjAxJqlrd_wAhUBLewKHYm4DbIQFjADegQIBRAD&url=https%3A%2F%2Fwww.agriland.ee%2Fmedia%2Fcom_eshop%2Fattachments%2FTrioliet_Solomix2_EN_2017-2018-web.pdf&usg=AOvVaw3-4TGhh1iQ_Mh0Nfi_KoO5>.

SOVA et al., 2014. Accuracy and precision of total mixed rations fed on commercial dairy farms. *Journal of Dairy Science*. vol. 97, issue 1, pp. 562-571. ISSN 0022-0302. [online]. Available at: <https://www.sciencedirect.com/science/article/pii/S0022030213007492>.

UNAL, H., KURALOGLU, H., 2015. Determination of operating parameters in milking robots with free cow traffic. *Engineering for Rural Development*, vol. 14, pp. 234-240. [online]. Available at: <https://www.researchgate.net/publication/280726826_Determination_of_operating_parameters_in_milking_robots_with_free_cow_traffic>.

Corresponding author:
Ing. Gabriel Lüttmerding, tel. +421 376 414 304, e-mail: xluttmerding@uniag.sk

VERIFICATION OF DECLARED DRIVING CHARACTERISTICS OF ELECTRIC VEHICLES IN REAL OPERATION

OVĚŘENÍ DEKLAROVANÝCH PROVOZNÍCH CHARAKTERISTIK ELEKTRICKÝCH VOZIDEL V REÁLNÉM PROVOZU

Štěpán Pícha, Veronika Štekerová, Martin Kotek, Veronika Hartová

Department of Vehicles and Ground Transport, Faculty of Engineering, Czech University of Life Sciences Prague, Kamýcká 129, Praha 6, Prague 16521, Prague, Czech Republic, pichas@tf.czu.cz

ABSTRACT: This paper is focused on the selected electric vehicles and their driving parameters. This paper tries to verify these declared driving parameters and draw conclusions from them. The selected vehicles drove the same predetermined route, which was 56,1 km long. The aim of this paper is to verify the operating parameters and driving characteristics of electric vehicles in real operation. The obtained data are used not only to verify the declared parameters of the manufacturer, but also to study factors that fundamentally affect these operating parameters. The obtained data differed from the declared 6.3 kWh/100 km of negative values to 5.7 kWh/100 km of positive values.

Key words: electric vehicles, operating parameters, real range, recuperation

ABSTRAKT: Publikace je zaměřena na vybraná elektrická vozidla a jejich jízdní parametry. Cílem tohoto dokumentu je ověřit deklarované provozní parametry a jízdní vlastnosti elektrických vozidel v reálném provozu a vyvodit z nich závěry. Vybraná vozidla jela po stejné předem stanovené trase, která byla dlouhá 56,1 km. Získané údaje byly použity nejen k ověření deklarovaných parametrů výrobcem, ale také ke studiu faktorů, které tyto provozní parametry zásadně ovlivňují. Získaná data se lišila od deklarovaných 6.3 kWh/100 km záporných hodnot do 5.7 kWh/100 km kladných hodnot.

Klíčová slova: elektrická vozidla, provozní parametry, reálný dojezd, rekuperace

INTRODUCTION

The constantly increasing number of vehicles is causing problems all around the world, whether it is traffic congestion, parking or, last but not least, air pollution. The vast majority of today‘s car uses an internal combustion engine, either gasoline or diesel. It is these engines that cause air pollution and make human lives uncomfortable in large urban agglomerations, where tens of thousands of these engines can run at once. Furthermore, the impending shortage of fossil fuels, along with the increasing environmental pollution in recent years have led to fundamental changes in the development of the automotive

industry. In everyday life, these changes can be felt mainly in the area of emission limits and the tightening of emission regulations for the entry of vehicles into selected cities. Exhaust emissions scandals have also played a role in short-term history, bringing with them, among other things, growing skepticism about internal combustion engines. Electromobility is currently considered to be an effective way to reduce the production of these harmful emissions from transport and thus prevent further environmental pollution and associated global warming (May, 2017).

According to the current EU Regulation no. 443/2009 are established emission performance standards for newly manufactured passenger cars as part of an integrated approach to reduce CO_2 emissions. The set emission limit for this regulation for newly manufactured vehicles is 130 g CO_2 per kilometer driven. Since 2020, this emission limit has been reduced to 95 g CO_2 per kilometer driven. If this limit is exceeded, there is a risk of financial penalties for manufacturers from 2019 (Domínguez-Navarro et al., 2019).

One of the consequences of the development during recent years is the ever-increasing sales of electric cars. These are considered to be the successor to cars with internal combustion engines. Many car manufacturers have announced in the near future the cessation of series production of vehicles with internal combustion engines. The reason is precisely the strict emission limits, the non-observance of which risks high fines for manufacturers. In this context, however, it is necessary not to forget the impact of the increase in electromobility on the electricity system and, if necessary, to implement appropriate measures (Anastasiadis et al., 2019) (Putrus et al., 2009).

Electromobility is one of the leading topics of today's, not only an energy industry. The growing using of electric cars in the world has been a continuing trend for several years and no change is expected in the upcoming years. For example, in Europe only, even more dynamic growth in the volume of electric cars is expected in the context of the European Commission's ambitious plans. Electric vehicles are characterized by the fact that their operation is locally emission-free and thus does not emit harmful CO_2 emissions into the air. In addition, if we consider that the electricity produced for their propulsion could in the future come exclusively from renewable energy sources (RES), we get a highly environmentally friendly mode of transport. Even if the energy produced from RES does not come, we have at least a more environmentally friendly mode of transport to large cities, as the production of emissions and dust particles will be reduced in densely populated areas. It is also true that electric vehicles are generally quieter and more efficient than cars with conventional motors (Klettke et al., 2018).

MATERIAL AND METHODS

The measurement of operating parameters of selected electric vehicles took place on a pre-selected route, which was completed by all vehicles. The measurement was performed using texa, bosch or vag-com diagnostic devices, which communicated with the electric drive control unit during the measurement, from which instantaneous values of operating parameters were obtained (especially battery voltage and current, state of charge, electric motor speed, vehicle speed).

These values were continuously recorded and stored by the system. In addition, the vehicles were equipped with a device for tracking the current position using the Garmin GPS 18x USB navigation unit.

Electric vehicles

For the purpose of analyzing the operating parameters of electric vehicles, several electric vehicles were rented:

- BMW i3s
- Škoda CITIGOe iV
- Fiat 500e
- Volkswagen ID.3

The technical parameters of selected electric vehicles are listed in Table 1. Figure 1-4 shows the tested electric vehicles which has been selected.

Table 1 Technical parameters of tested electric vehicles
Tabuľka 1 Techické parametre testovaných elektrických vozidiel

	Weight	Torque	Engine power	Battery weight	Battery capacity	Range	Maximal speed	Consumption per 100 km
Vehicle	(kg)	(Nm)	(kW)	(kg)	(kWh)	(km)	(km·h^{-1})	(kWh)
BMW i3s	1 365	270	135		42 (38)	300	160	13,1
CITIGOe iV	1 530	212	61	248	36,8	252	130	14,8
Fiat 500e	1 352	200	83	260	24	135	142	18
VW ID3	1719	310	150		58	420	160	16,1

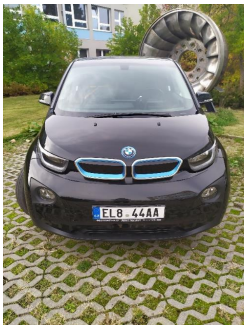
Fig.1 BMW i3s


Fig.2 CITIGOe iV


Fig.3 Fiat 500e

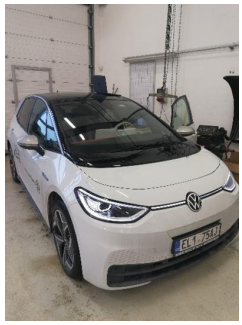
Fig.4 Volkswagen ID. 3

Instrumentation

The instrumentation used in the test runs with electric vehicles is described in the following subsections. These were mainly TEXA, VAG-COM and BOSCH diagnostic devices for communication with the control units in the vehicle and storing the available instantaneous operating parameters.

TEXA diagnostic TXTs

The Texa diagnostic unit is intended for multi-brand serial diagnostics of passenger cars. It also allows monitoring and evaluation of measured values from the car‘s control units in real time. It can only be used to diagnose passenger cars with an OBD diagnostic socket. This socket is available to all vehicles from the year of manufacture 2000. The IDC3 Pocket software only makes vehicles equipped with an OBD socket available. The device is therefore connected to the vehicle‘s diagnostic socket and uses Bluetooth to communicate between the vehicle and the display unit (PC or PDA). Thanks to continuous measurement, it is possible to monitor the characteristics of the engine while driving (*NAVIGATOR TXTs - Diagnostics for all environments - TEXA S.p.A.*, 2021).

Diagnostic system Vag-COM (HexCAN-V2)

This diagnostic device enables communication with group cars (VW, Audi, Seat, Škoda) using the HexCan-V2 communication interface (Fig. 12) and the VAG-COM computer program, which is intended for vehicle diagnostics via serial diagnostics. The software allows you to view and save instantaneous values of operating parameters by connecting to the appropriate vehicle control unit (*Autodiagnostika VCDS 20.4.1 VAG-COM HEX-V2*, 2021).

BOSCH KTS 590

Bosch KTS 590 diagnostics can be seen in Figure 13. These are control equipment, diagnostics, troubleshooting the electronic control systems of modern petrol and diesel engines, including ABS, ASR, ESP, automatic transmission control, comfort control and security systems and many more. This device, together with the ESI-Tronic software, allows many diagnostic tasks to be performed on the vehicle. Diagnostic tasks include, for example, reading the fault memory, clearing the fault memory, monitoring the measured values, performing an actuator test, resetting the service intervals or, for example, communicating with the EOBD control units. The KTS 590 diagnostic tool has an integrated two-channel oscilloscope and a multimeter for measuring voltage, resistance and current. It can be connected to a personal computer using a USB cable or Bluetooth wireless technology (*KTS 590 | Bosch Automotive aftermarket Česká republika*, 2021).

GPS Garmin

A Garmin GPS-18x USB satellite receiver was used to capture the current position of vehicles, and an application for recording instantaneous values from a GPS sensor was created in the ControlWeb environment.

Test route

The test route was based on the WLTP (World Harmonized Light-duty Procedure) vehicle type-approval regulation, in particular the RDE (Real Driving Emissions) part. The test route must include urban, extra-urban and motorway traffic according to precise specifications, which further define the achieved average speed, route elevation, route timing, climatic conditions and more. The total length of the route was 56.1 km. The proposed test route was always driven in both directions. The starting point for the start of the ride was the CULS TF workshops.

The following figure (Fig. 5.) shows the selected test route. The orange part shows city traffic (CULS-Letňany, Kralupy nad Vltavou), dark blue extra-urban traffic (CULS-Kralupy nad Vltavou) and light blue motorway traffic (Kralupy nad Vltavou-Letňany).

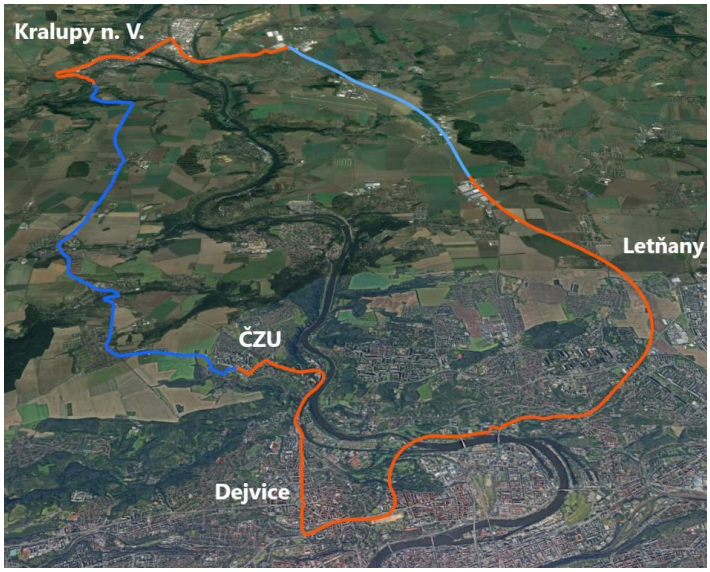

Fig. 5 Test route
Obr. 5 Testovacia trať

RESULTS

Table 2. Summarizes the basic results of the performed experiments. The aim of the measurement was to verify the declared range of selected electric vehicles in real operation. During the measurement, it was not possible to establish communication between the

vehicle control unit and the diagnostic device in some vehicles. Alternatively, the connection was not reliable and data was lost.

The average speed of vehicles was affected only by the immediate traffic situation, as the defensive driving style and compliance with traffic regulations. The achieved average speed of the tested vehicles ranges from 40 to 47 km/h and did not show significant fluctuations. In the case of the BMW i3s, the measured consumption value was by 0.8 kWh/100 km higher than declared. On the other hand, the Škoda CITIGOe iV and Fiat 500e showed lower electricity consumption. Analogic values were, in the case of the Škoda CITIGOe iV 2.2 kW/100 km and in the case of the Fiat 500e by up to 5.7 kWh/100 km. The highest electricity consumption was achieved by the VW ID3 vehicle, namely 22.4 kWh/100 km, is 6.3 kWh/100 km – higher than the declared value.

Table 2 Basic summary results
Tabuľka 2 Základné sumárne výsledky

	Declared energy consumption	**Average consumption during the test**	**The difference between declared consumption and measured consumption**	**Average speed**	**Date**	**Outside temperature**
Vehicle	kWh/100 km	kWh/100 km	kWh/100 km	km/h	–	**°C**
BMW i3s	13,1	13.9	0.8	46	13.01.2021	1
CITIGOe iV	14,8	12.6	2.2	42	14.10.2020	6.5
Fiat 500e	18	12.3	5.7	40	21.10.2020	12
VW ID3	16,1	22.4	6.3	47	11.02.2021	–10

DISCUSSION

At present, we can see societal pressure to reduce the negative impact on the environment when using internal combustion engines. The study by Bloomberg New Energy Finance (BNEF) states that carmakers are accelerating their marketing plans, in part to comply with increasingly stringent regulations in Europe and China. COVID-19 will delay some of them, but by 2022, more than 500 different EV models will be available worldwide. Consumer choice and competitive prices will be key to attracting new buyers to the market (McKerracher et al., 2021). It is the verification of the range of individual vehicles that is crucial for determining the relevance of the mentioned parameters of electric vehicles.

Releasing of electric energy from batteries is one of crucial parameters which influence final power supply. Our results show that in the case of the BMW i3s and Škoda CITIGOe iV vehicles, there were no significant fluctuations in electricity consumption from the declared values specified by the vehicle manufacturer. Even at relatively low outside temperatures. That means the power supply is fluent and predictable and this information increases the confidence for these cars.

On the other hand, there was a difference in consumption for the Fiat 500e, but the measured value was 5.7 kWh/100 km lower than stated by the vehicle manufacturer. Dif-

ferent effect could be source of this phenomenon the most probable appears to be the traffic situation during this measurement had an effect on the final consumption, which is evident from the lower average speed (40 km/h).

In the case of the VW ID3, the measured consumption of the vehicle was 6.3 kWh/100 km higher than declared. In this case, it was probably the fact that the outside temperature during the measurement was -10 ° C. In other experiments was verified the low temperature can affect the capacity of the battery located in the vehicle (The lower capacity of the batteries at low temperatures is stated in a study carried out by the Norwegian Automobile Federation (NAF)(*20 popular EVs tested in Norwegian winter conditions | NAF*, 2020)). Information of such tape is very important for users and customers in relevant climatic conditions.

CONCLUSION

As part of the verification of the declared parameters by the manufacturer, a total of 4 electric vehicles were tested, some even repeatedly (according to the immediate situation and availability of cars). For the time being, there is still the problem of complex sensing of the instantaneous operating parameters of the electric drive, or the electric vehicle as a whole. Direct connection of the electric drive by external measuring devices is impossible, mainly for safety reasons, where the operating voltage is 400 V and the current taken from the batteries reaches the order of hundreds of amperes. For this reason, diagnostic devices are used to read and obtain parameters, which can be connected via the diagnostic socket. However, the availability of data itself often depends on the vehicle manufacturer or its age. The manufacturer of the diagnostic tool also plays a role. Although it can be connected to the correct control unit (usually an electric drive unit), there is no guarantee that there will be an instantaneous value of current and voltage on the high-voltage battery or electric motor, from which the actual electricity consumption can then be calculated.

Despite these difficulties, during the measurement it was confirmed that the data of the operating parameters of the vehicles, which are verified during the homologation procedure (according to the new WLTP methodology), correspond to great extent to real traffic. However, some fluctuations were recognized. The general traffic, for instance, that had led to lower average speed had reasonable effect on reduction of energy consumption how it can be seen on example of Fiat 500e. The instantaneous climatic conditions could be the explanation of higher energy consumption in the case of the VW ID3 and contemporary it was the biggest and the heaviest from tested vehicles.

Experiments have shown that the declared range of vehicles was in general verified in real traffic. Although, the real climatic conditions, traffic situation or driving style of the driver had additional significant effect.

ACKNOWLEDGMENT

The work was supported by the internal research project of Czech University of Life Sciences Prague of Faculty of Engineering IGA 2020:31150/1312/3102.

REFERENCES

ANASTASIADIS, A. G., KONDYLIS, G. P., POLYZAKIS, A., VOKAS, G. 2019. Effects of increased electric vehicles into a distribution network. In: *Energy Procedia* [online]. B.m.: Elsevier Ltd, 2019, p. 586–593. ISSN 18766102. Available on: doi:10.1016/j.egypro.2018.11.223

DOMÍNGUEZ-NAVARRO, J. A., DUFO-LÓPEZ, R., YUSTA-LOYO, J. M., ARTAL-SEVIL, J. S., BERNAL-AGUSTÍN, J. L. 2019. Design of an electric vehicle fast-charging station with integration of renewable energy and storage systems. *International Journal of Electrical Power and Energy Systems*, **105**, pp. 46–58. ISSN 01420615. Available on: doi:10.1016/j.ijepes.2018.08.001

KLETTKE, A., MOSER, A., BOSSMANN, T., BARBERI, P., FOURNIÉ, L. 2018. *Effect of electromobility on the power systeam and the integration of RES* [online]. 2018 [cit. 2021-07-03]. Available on: http://europa.eu

KTS 590 | Bosch Automotive aftermarket Česká republika [online]. 2021 [vid. 2021-07-03]. Available on: https://www.boschaftermarket.com/cz/cs/diagnostika/tester-pro-diagnostiku-řídicích-jednotek/kts-nastroje-pro-diagnostiku/kts-590/

MAY, N. 2017 Local environmental impact assessment as decision support for the introduction of electromobility in urban public transport systems. *Transportation Research Part D: Transport and Environment*, **64**(July 2017), pp. 192–203. ISSN 13619209. Available on: doi:10.1016/j.trd.2017.07.010

MCKERRACHER, C., O'DONOVAN, A., ALBANESE, N., SOULOPOULOS, N., DOHERTY, D., BOERS, M., FISHER, R., CANTOR, C., FRITH, J., MI, S., GRANT, A., LYU, J., AMPOFO, K., ABRAHAM, A. 2021. *EVO Report 2021 | BloombergNEF | Bloomberg Finance LP* [online]. [cit. 2021-07-03]. Available on: https://about.bnef.com/electric-vehicle-outlook/

NAVIGATOR TXTs - Diagnostics for all environments - TEXA S.p.A. [online]. 2021 [vid. 2021-07-03]. Available on: https://www.texa.com/products/navigator-txts

PUTRUS, G. A., SUWANAPINGKARL, P., JOHNSTON, D., BENTLEY, E. C., NARAYANA, M. 2009. Impact of electric vehicles on power distribution networks. In: *5th IEEE Vehicle Power and Propulsion Conference, VPPC '09*, pp. 827–831. ISBN 9781424426003. Available on: doi:10.1109/VPPC.2009.5289760

Autodiagnostika VCDS 20.4.1 VAG-COM HEX-V2 [online]. 2021 [vid. 2021-07-03]. Available on: http://www.vag-com.cz/

20 popular EVs tested in Norwegian winter conditions | NAF [online]. 2020 [vid. 2021-06-11]. Available on: https://www.naf.no/elbil/aktuelt/elbiltest/ev-winter-ran;;ge-test-2020/

Corresponding author:
Ing. Štěpán Pícha, e-mail: pichas@tf.czu.cz

INFLUENCE OF DEFORMATION RATE ON THE STRENGTH OF POLYMER COMPOSITE MATERIAL WITH FILLER BASED ON WOOD POWDER INTENDED FOR ADDITIVE TECHNOLOGIES

VPLYV RÝCHLOSTI DEFORMÁCIE NA PEVNOSŤ POLYMERNÉHO KOMPOZITNÉHO MATERIÁLU S PLNIVOM NA BÁZE DREVENÝCH PILÍN URČENÝCH PRE ADITIVNE TECHNOLÓGIE

Dominik Piš[1]; Hana Pouzarová[2]

[1]Department of Material Science and Manufacturing Technology, Faculty of Engineering, Czech University of Life Sciences Prague, Kamycka 129, Prague 6 – Suchdol, 165 00 Prague, Czech Republic; pisd@tf.czu.cz
[2]Department of Material Science and Manufacturing Technology, Faculty of Engineering, Czech University of Life Sciences Prague, Kamycka 129, Prague 6 – Suchdol, 165 00 Prague, Czech Republic; pouzarova@tf.czu.cz

ABSTRACT: The article deals with the influence of the strain rate on the strength of a polymer composite material with a filler based on wood powder intended for additive technologies. The aim of the article is to compare the influence of the strain rate on the maximum stress and elongation of the composite material. The tensile test was performed on the universal testing machine LabTest 5.50ST type (LaborTech, Opava, Czech Republic) was performed for 6 different deformation speeds (1 mm / min, 2.5 mm / min, 5 mm / min, 10 mm / min, 15 mm / min and 20 mm / min). The maximum strength limit reached was 34.19 MPa at a strain rate of 20 mm / min and the minimum strength limit was 27.37 MPa at a strain rate of 1 mm / min. The maximum elongation was 4.35 mm at 1 mm / min and the minimum elongation was 2.55 mm at 20 mm / min. Significant porosity of the material was found by microscopic analysis of the ruptured material.

Keywords: 3D printing, strain rate, bio-composite, PLA, mechanical properties, tensile strength

ABSTRAKT: Článek se zabývá vlivem rychlosti deformace na pevnost polymerního kompozitního materiálu s plnivem na bázi dřevěných pilin určených pro aditivní technologie. Cílem článku je porovnat vliv rychlosti deformace na maximální napětí a prodloužení kompozitního materiálu. Tahová zkouška na univerzálním zkušebním stroji LabTest 5.50ST type (LaborTech, Opava, Česká republika) byla provedena pro 6 různých deformačních rychlostí (1 mm/min, 2.5 mm/min, 5 mm/min, 10 mm/min, 15 mm/min a 20 mm/min). Byla zjištěna maximální mez pevnosti 34.19 MPa při rychlosti deformace 20 mm/min a minimální mez pevnosti 27.37 MPa při rychlosti deformace 1 mm/min a maximální prodloužení 4.35 mm při rychlosti 1 mm/min a minimální prodloužení 2.55 mm při

rychlosti 20 mm/min. Při mikroskopické analýze přetrženého materiálu byla zjištěna značná pórovitost materiálu.

Klíčová slova: 3D tisk, rychlost deformace, biokompozit, PLA, mechanical properties, tensile strength

INTRODUCTION

The market for polymer composites with wood-based fillers is growing, especially in the automotive and construction industries (Jeske et al. 2012). Wood particles for polymer composite are used mainly due to their low density, mechanical properties, ecological nature and low cost (Farsi 2010). In Europe in 2012, the total volume of production wood-based polymer composites was 260,000 tons (Wood Plastic Composites 2012). Majority wood-based polymer composites are made from oil-based polymers, which include polyethylene, polyvinyl chloride, polypropylene and etc (Friedrich 2018, Espert et al. 2004). Oil-based polymers are only partially biodegradable and difficult to recycle. with regard to the environment, efforts are being made to replace them with biopolymers (Spear et al. 2015, Robledo-Ortíz et al. 2012).

A very perspective biopolymer is polylactic acid (PLA) and polyhydroxybutyrate (PHB); both of these polymers are biodegradable (on an industrial scale) and used extensively in industry (Guo et al. 2018, Torres-Tello et al. 2017). PLA is made from lactic acid monomer, which is obtained by fermentation of corn, potatoes or sugar beet. These are majority often the synthesis and polymerization of lactides (Briassoulis 2016, Zhang et al. 2017).

These biopolymers have some significant disadvantages, such as low resistance to higher temperatures and brittleness; the properties of these polymers can be modified by mixing them or by using different fillers; for example Arrieta et al. (2015) states an increase in tensile strength of up to 100% in a PLA / PHB mixture with a weight ratio of 50/50. However, the disintegration rate of this mixture was lower than that of pure polymers.

The growing market for biopolymers has made these polymers more availability, but they still have higher production costs than conventional polymers. Achieving lower end costs can be achieved by combining biopolymers with low-cost materials; such material may be wood particles. Petinakis et al. (2009) states that the addition of 20% by weight of wood particles to the PLA polymer slightly reduced the tensile strength from 60 MPa to 57 MPa. Pérez-Fonseca et al. (2016) observed a decrease in tensile strength from 60 MPa to 48 MPa and from 95 to 63 MPa in bending in bio-composites with a matrix of PLA and 30% of filler weight from pine powder. Also Pilla et al. (2008) states that the addition of 20% and 40% by weight of wood content reduced the tensile strength of PLA from 55 MPa to 54 MPa and 51 MPa, while 40% by weight of silane-treated wood particles increased the tensile strength of PLA up to 57 MPa. Young›s modulus of elasticity of materials increased in both treated and untreated wood particles, at both studied concentrations (Pilla et al. 2008). Reduction of tensile strength is common with wood-base composite polymers; it largely depends on the percentage of wood particles and their modification (Csikós et al. 2015).

The speed and type of loading is important for the characterization of polymers because polymers react non-linearly to mechanical loads; for this reason, the material properties of polymers are highly dependent on the loading rate (Richeton et al. 2006). Petersmann et al. (2020) observed the effect of strain rate on various materials intended for 3D printing. As a result, most materials achieved different tensile strengths and ductility at different loading speeds. Majority of materials achieved higher tensile strengths and less strain at break at higher strain rates; PLA and PP did not have a large dependence of mechanical properties on the rate of deformation compared to other polymers such as PETG, PEEK and PMMA.

The aim of the experiment was to compare the effect of material deformation rate on material strength and specific elongation in test specimens made of PLA with wood powder printed using FDM 3D printing technology.

MATERIAL AND METHODS

The test specimens are made of a filament of PLA polymer with 20% by weight of wood powder filler. The used filament was made by SUNLU INDUSTRIAL CO., LTD. The manufacturer does not state the origin, size of the wood filler, or whether the filler has been modified.

The test specimens were made by 3D printer Prusa i3 MK3S+. To avoid the risk of blockage of the nozzle by filament, a nozzle with a diameter of 1 mm was used. The layer height was 0.2 mm, other print settings were 3 outer perimeters, 100% straight fill at an angle of 45° to the X axis, print speed 80 mm/s with deceleration to 50 mm/s on the outer perimeter and top layer fill and 25 mm/s to print the first layer. The printing nozzle temperature was set to 200 °C and the hot bad temperature was 50 °C. The cooling fan speed was 20%. During one print, 8 pieces were made. test specimens. The test specimens were oriented longitudinally to the X-axis during printing. A total of 42 test specimens were printed.

The tensile test was performed according to the ČSN EN ISO 527–2 standard, according to which type 1 B test specimens were print. The tensile test was performed on the universal testing machine of the LabTest 5.50ST type (LaborTech, Opava, Czech Republic). The test was performed for 6 tensile strain rates - 1 mm/min, 2.5 mm/min, 5 mm/min, 10 mm/min, 15 mm/min and 20 mm/min. 7 test specimens were used for each speed.

RESULT AND DISCUSSION

Figure 1 shows that the tensile strength has an increasing tendency with increasing strain rate of the tensile test. The maximum average stress achieved during the experiment was reached at a strain rate of 20 mm/min.

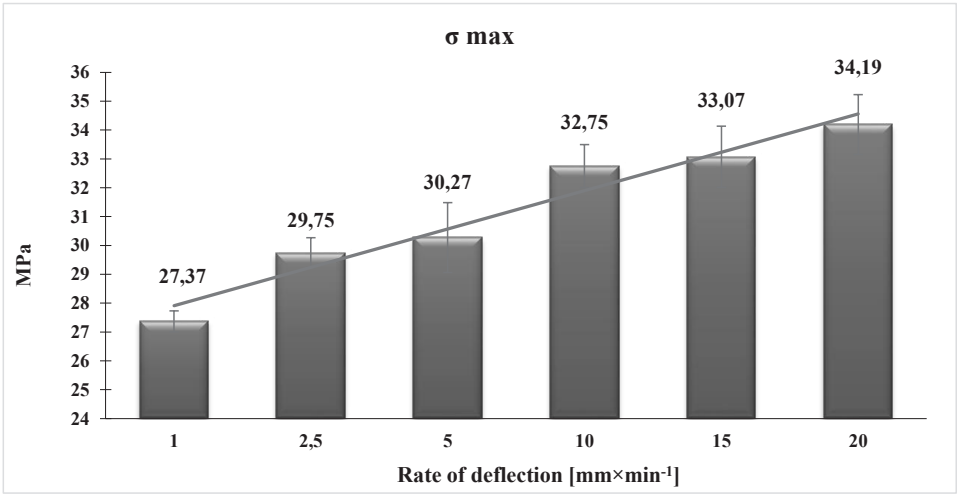

Fig. 1 Tensile strength
Obr. 1. Ťahové napätie

Figure 2 shows that the maximum elongation has a decreasing tendency with increasing strain rate of the tensile test. The maximum average elongation achieved during the experiment was reached at a strain rate of 1 mm/min.

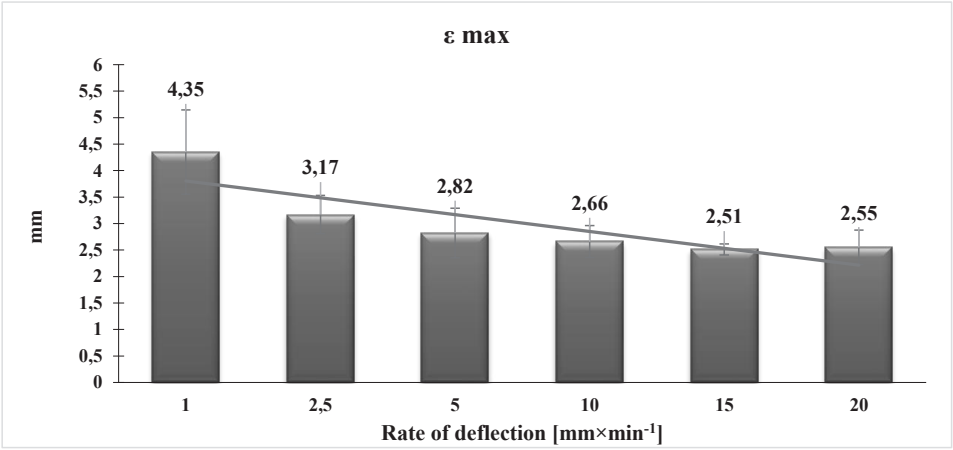

Fig. 2 Elongation
Obr. 2 Predĺženie

Figure 3 shows the fracture surface of the test specimen. The figure shows considerable porosity and the presence of air bubbles. The presence of air gaps can be caused by the content of air bubbles already in the filament, by the moisture of the material during printing or by sucking air into the nozzle during the retraction of the filament during printing.

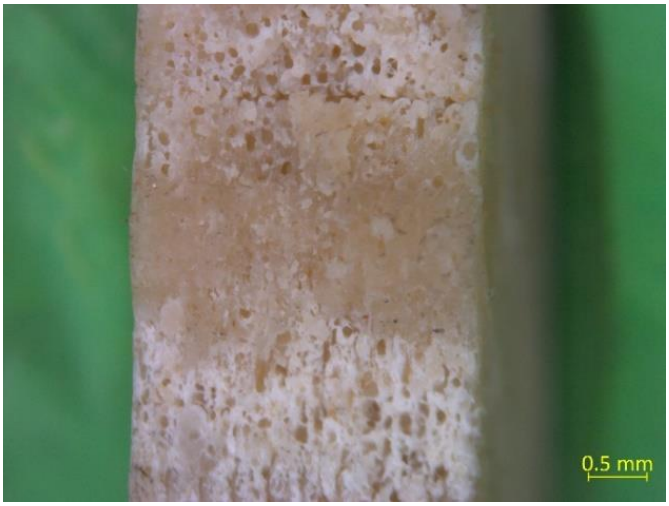

Fig. 3 Fracture surface of the test specimen
Obr. 3 Lomová plocha skúšobnej vzorky

M. S. Huda et al. (2006) reports almost twice the tensile strength of PLA polymer with a 20 % wood sawdust content of 65.7 MPa for injection molding test specimens. The maximum tensile strength achieved during the experiment was 34.19 MPa. Different values may be due to the method used to manufacture the test specimens, as air bubbles formed during preparation on the 3D printer, which affected the strength of the material. The measured values of the experiment correspond to the statement that with increasing deformation rate the strength of the material increases, but achieves lower ductility compared to slower types of deformation. Petersmann et al. (2020).

CONCLUSION

The aim of the article was to compare different strain rates for PLA test specimens with wood powder made by additive 3D printing technology. The results of the article show that the maximum stress of 34.19 MPa was reached at a speed of 20 mm/min. The maximum elongation of 4.35 mm was reached at a speed of 1 mm/min. The rate of deformation affects the maximum strength of the material and the elongation. The reduced strength of the material in 3D printing could be caused by air pores inside the material. These pores could have formed for various reasons.

ACKNOWLEDGMENT

Contribution has been prepared within the solving of scientific grant project IGA 2021:31140/1312/3115 "Degradation of polymer composite materials printed by 3D printing with cellulose-based filler."

REFERENCES

ARRIETA, M. P., LÓPEZ, J., LÓPEZ, D., KENNY, J. M., PEPONI, L. Development of flexible materials based on plasticized electrospun PLA-PHB blends: Structural, thermal, mechanical and disintegration properties. *European Polymer Journal*, 73, pp. 433–446.

BRIASSOULIS, D. 2016. Mechanical behaviour of biodegradable agricultural films under real field conditions. *Polymer Degradation and Stability*, 91(6), pp. 1256–1272.

CSIKÓS, Á., FALUDI, G., DOMJÁN, A., RENNER, K., MÓCZÓ, J., PUKÁNSZKY, B. 2015. Modification of interfacial adhesion with a functionalized polymer in PLA/wood composites. *European Polymer Journal*, 68, pp. 592–600.

ESPERT, A., VILAPLANA, F., KARLSSON, S. 2004. Comparison of water absorption in natural cellulosic fibres from wood and one-year crops in polypropylene composites and its influence on their mechanical properties. *Composites Part A: Applied Science and Manufacturing,* 35(11), pp. 1267–1276.

FARSI, M. (2010). Wood-plastic composites: Influence of wood flour chemical modification on the mechanical performance. *Journal of Reinforced Plastics and Composites,* 29(24), 3587–3592.

FRIEDRICH, D. 2018. Comparative study on artificial and natural weathering of wood-polymer compounds: A comprehensive literature review. *Case Studies in Construction Materials*. 9, e00196.

GUO, R., REN, Z., BI, H., SONG, Y., XU, M. 2018. Effect of toughening agents on the properties of poplar wood flour/poly (lactic acid) composites fabricated with Fused Deposition Modeling. *European Polymer Journal*, 107, pp. 34–45.

HUDA, M. S., DRZAL, L. T., MISRA, M., MOHANTY, A. K. 2016. Wood-fiber-reinforced poly(lactic acid) composites: Evaluation of the physicomechanical and morphological properties. *Journal of Applied Polymer Science*, 102(5), pp. 4856–4869.

JESKE, H, SCHIRP, A., CORNELIUS, F. 2012. Development of a thermogravimetric analysis (TGA) method for quantitative analysis of wood flour and polypropylene in wood plastic composites (WPC). *Thermochimica Acta*, 543, pp. 165–171.

PÉREZ-FONSECA, A. A., ROBLEDO-ORTÍZ, J. R., GONZÁLEZ-NÚÑEZ, R., RODRIGUE, D. 2016. Effect of thermal annealing on the mechanical and thermal properties of polylactic acid–cellulosic fiber biocomposites. *Journal of Applied Polymer Science*, 133(31).

PETERSMANN, S., SPOERK, M., VAN DE STEENE, W., ÜÇAL, M., WIENER, J., PINTER, G., ARBEITER, F. 2020. Mechanical properties of polymeric implant materials produced by extrusion-based additive manufacturing. *Journal of the Mechanical Behavior of Biomedical Materials*, 104, 103611.

PETINAKIS, E., YU, L., EDWARD, G., DEAN, K., LIU, H., SCULLY, A. D. 2009. Effect of matrix-particle interfacial adhesion on the mechanical properties of poly(lactic acid)/wood-flour micro-composites. *Journal of Polymers and the Environment*, 17(2), pp. 83–94.

PILLA, S., GONG, S., O'NEILL, E., ROWELL, R. M., KRZYSIK, A. M. 2008 Polylactide-pine wood flour composites. *Polymer Engineering and Science*, 48(3), pp. 578–587.

RICHETON, J., AHZI, S., VECCHIO, K. S., JIANG, F. C., ADHARAPURAPU, R. R. 2006. Influence of temperature and strain rate on the mechanical behavior of three amorphous polymers: Characterization and modeling of the compressive yield stress. *International Journal of Solids and Structures*, 43(7–8), pp. 2318–2335.

ROBLEDO-ORTÍZ, J. R., GONZÁLEZ-LÓPEZ, M. E., MARTÍN DEL CAMPO, A. S., PÉREZ-FONSECA, A. A. 2021. *Lignocellulosic Materials as Reinforcement of Polyhydroxybutyrate and its Copolymer with Hydroxyvalerate: A Review*. B.m.: Springer. May, 01. 2021

SPEAR, M. J., EDER, A., CARUS, M. 2015. Wood polymer composites. *Wood Composites*. B.m.: Elsevier Inc., 2015, pp. 195–249. ISBN 9781782424772.

TORRES-TELLO, E. V., ROBLEDO-ORTÍZ, J. R., GONZÁLEZ-GARCÍA, Y., PÉREZ-FONSECA, A. A., JASSO-GASTINEL, C. F. MENDIZÁBAL., E. 2017. Effect of agave fiber content in the thermal and mechanical properties of green composites based on polyhydroxybutyrate or poly(hydroxybutyrate-co-hydroxyvalerate). *Industrial Crops and Products*, 99, pp. 117–125.

Wood-Plastic Composites (WPC) and Natural Fibre Composites (NFC): European and Global Markets 2012 and Future Trends - Renewable Carbon. Dostupné z: http://bio-based.eu/downloads/wood-plastic-composites-wpc-and-natural-fibre-composites-nfc-european-and-global-markets-2012-and-future-trends-in-automotive-and-construction-2/

ZHANG, L., LV, S., SUN, C., WAN, L., TAN, H., ZHANG, Y. 2017. Effect of MAH-g-PLA on the Properties of Wood Fiber/Polylactic Acid Composites. *Polymers*, 9(11), pp. 591.

Corresponding author:
Dominik Piš, pisd@tf.czu.cz

ABRASION RESISTANCE OF MODIFIED SNOW PLOUGHSHARE MATERIALS

ABRAZÍVNA ODOLNOSŤ MATERIÁLOV UPRAVENEJ SNEŽNEJ RADLICE

Monika Vargová[1], Miroslava Ťavodová[2]

[1,2]Department of Manufacturing Technology and Quality Management, Faculty of Technology, Technical University in Zvolen, Študentská 26, 960 01 Zvolen
e-mail: [1]monika.vargova@tuzvo.sk, [2]tavodova@tuzvo.sk

ABSTRACT: The article presents abrasion resistance study results of a modified snow ploughshare materials. The material HARDOX 450 was chosen as the etalon sample. Snow ploughshare ranking blade is made from HARDOX 450. Weld deposit OK 84.58 was chosen as a reference sample. Weld deposit was applied to a part of the discarded snow ploughshare. The test was performed according to the Russian standard GOST 23.208-79. Subsequently the relative abrasion resistance and the hardness coefficients were calculated. Based on this test, we can state that the sample with the OK 84.58 weld deposit achieved 24% better resistance to abrasive wear, compared to the sample made from HARDOX 450 material. The hardness coefficients of the etalon sample and the reference sample also confirm that the weld deposit OK 84.58 can better withstand abrasive particles than the material HARDOX 450. As the raking blades are exposed to high wear during their operation, especially abrasive, and their change is relatively economically arduous, it is necessary to look for ways to increase their service life and examine their resistance to abrasive wear.

Key words: abrasive wear, abrasion resistance test, ploughshare, HARDOX

ABSTRAKT: V článku sú predstavené výsledky skúmania abrazívnej odolnosti materiálov upravenej snežnej radlice. Za etalónovú vzorku bol zvolený materiál HARDOX 450. Z HARDOX 450 sa vyrábajú aj zhrňovacie nože snežných radlíc. Za porovnávaciu vzorku bola zvolená vzorka s návarom OK 84.58. Tento návar bol aplikovaný na časť vyradenej snežnej radlice. Skúška bola vykonaná podľa ruskej normy GOST 23.208-79. Následne sa vypočítala pomerná odolnosť voči abrazívnemu opotrebeniu a koeficienty tvrdostí . Na základe tejto skúšky môžeme konštatovať, že vzorka s návarom OK 84.58 dosiahla o 24% lepšiu abrazívnu odolnosť, v porovnaní so vzorkou z materiálu HARDOX 450. Koeficienty tvrdostí etalónu a porovnávacej vzorky taktiež potvrdzujú, že návar OK 84.58 dokáže lepšie odolávať abrazívnym časticiam ako materiál HARDOX 450. Snežné radlice sú pri svojej práci vystavené vysokému opotrebeniu, a to hlavne abrazívnemu a ich výmena je pomerne ekonomicky náročná. Preto je potrebné hľadať možnosti zvyšovania ich životnosti a skúmať ich odolnosť voči abrazívnemu opotrebeniu.

Kľúčové slová: abrazívne opotrebenie, skúška oteruvzdornosti, radlica, HARDOX

INTRODUCTION

The most common undesirable phenomenon in industry is wear, which leads to the replacement of parts, components, and tools. Wear is the process of gradually losing material from the surface of a material (Sabet *et al.,* 2011). There are several types of wear, namely adhesive, abrasive, erosive, corrosive and fatigue wear (Findik, 2014).

The most dominant type of wear is abrasive wear (Singh *et al.,* 2020 a,b). It is assumed that abrasive wear is responsible up to 50% of failures, respectively decommissioning of parts, components, and tools (Blau and Dehoff, 2013; Vencl *et al.,* 2010). The wear mechanism is a complex process in the context of many factors. The intensity of these factors depends on the operating conditions of the environment, where are the components and tools exposed during their operation, and the operating parameters of machines and the material properties of contact surfaces (Suchánek *et al.,* 2009).

Wear caused by shocks and abrasion of hard abrasive particles is a major problem in many industries, especially in the areas of forestry, mining, mineral processing, etc. (Ťavodová *et al.,* 2020; Zdravecká *et al.,* 2014).

Snow ploughshares, which are used to ensure the passability of forest roads, are exposed to unfavourable working conditions in the process of their work. They are subject to wear, especially abrasive, as they work in a heterogeneous environment. Due to their rapid wear, they are taken out of service early, which causes technical and economic problems. For this reason, it is necessary to look for ways to increase their service life and examine their resistance to abrasive wear.

MATERIAL AND METHODS

The snow ploughshare was modified by hard surfacing the OK 84.58 electrode. Electrode OK 84.58 is a hard surfacing electrode depositing a semi-corrosion-resistant martensitic steel (Vargová and Ťavodová, 2020). Full hardness is obtained in the first bead, irrespective of the cooling rate. Hard surfaced parts are suitable for exposure to abrasive and impact wear, used in farm equipment, forestry tools, loading machines and mixers. The weld deposit can be machined by grinding (www.esab.com). Table 1 contains chemical composition of the electrode OK 84.58. This electrode was welded on a part of the discarded ploughshare.

Table 1 Chemical composition of the OK 84.58 electrode (www.esab.com)
Tabuľka 1 Chemické zloženie elektródy OK 84.58 (www.esab.com)

Element[1]	C	Si	Mn	Cr	Fe
wt.[2] [%]	0.7	0.6	0.7	10.0	rest

[1]Prvok; [2]hm.

We compared the abrasion resistance of the OK 84.58 weld deposit with the abrasion resistance of the HARDOX 450 material. HARDOX 450 is an abrasion-resistant steel with excellent construction properties. The hardness of this steel is 450 HBW, yield strength 1,100 MPa to 1,300 MPa. HARDOX 450 is well flexible and has guaranteed weldability. Provides good abrasion resistance and longer life. It is used in various components and constructions that are exposed to wear (www.gamaocel.cz). Based on the available information, HARDOX 450 is also used as a material for ranking blades (www.zbyneklazar.cz). For this reason, HARDOX 450 was chosen as an etalon sample. Table 2 contains chemical composition of the HARDOX 450 material.

Table 2 Chemical composition of the HARDOX 450 material (www.ssab.com)
Tabuľka 2 Chemické zloženie metriálu HARDOX 450 (www.ssab.com)

Element[1]	C	Si	Mn	P	S	Mo	Ni	Cr	B	Fe
wt.[2] [%]	max. 0.23	max. 0.50	max. 1.60	max. 0.025	max. 0.010	max. 0.25	max. 0.25	max. 1.20	max. 0.005	rest

[1]Prvok; [2]hm.

The abrasion resistance test was performed according to the Russian standard GOST 23.208-79. This standard is from the group of Ensuring the resistance of products to wear standards. The basis of the method is to compare the weight loss of reference sample and the weight loss of etalon sample under the same test conditions. In Fig. 1 is a device for testing the abrasion resistance of a material according to the Russian standard GOST 23.208-79 is presented. Electro corundum with a grain size of 16-P and relative moisture content of at most 0.15% was chosen as abrasive material. Its hardness corresponds to the 9th degree of the Mohs scale. When evaluating the resistance to wear under specific wear conditions, abrasive material corresponding to the material used during operation, but with a grain size up to 1.0mm can be used.

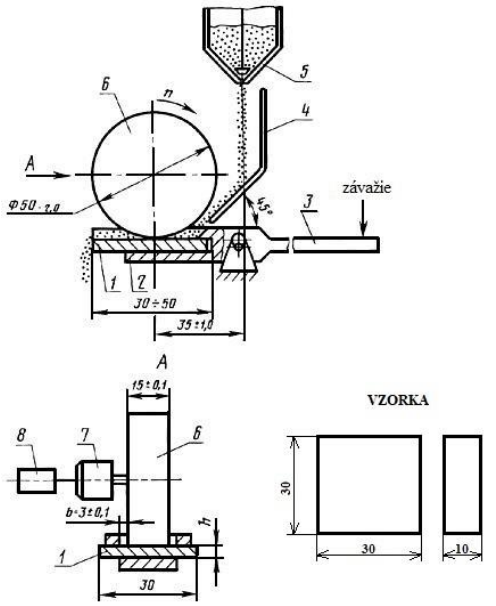

Fig. 1 Schematic of abrasion resistance test device according to GOST 23.208-79
1-sample, 2-sample holder, 3-lever, 4-rectifier of abrasive particles into the friction zone, 5-hopper, 6-rotating rubber disc, 7-actuation, 8- a device for checking a total number of speeds during the test
Obr. 1 Schéma prístroja pre skúšku oteruvzdornosti podľa GOST 23.208-79
1-vzorka, 2-držiak vzorky, 3-páka, 4-usmerňovač abrazívnych častíc do zóny trenia, 5-násypka, 6-rotujúci gumený valec, 7-pohon, 8-zariadenie pre kontrolu celkového počtu otáčok valca počas skúšky

Each test sample (etalon, reference sample) is weighed (min. 2x) and placed in the test device before the test. Subsequently, the abrasive supply (4, 5) is started, and the rubber disc (6) is pressed against the test sample (1). After completion of set track, the sample is taken and weighed again. The arithmetic mean is calculated from the determined weight losses of the individual measurements of the etalon and the reference sample.

The relative resistance to abrasive wear is calculated from equation 1.1:

$$\Psi_{abr} = \frac{W_{hE}}{W_{hR}} [-] \tag{1.1}$$

where: W_{hE} – weight loss of the etalon sample [g]
W_{hR} – weight loss of the reference sample [g]

Hardness coefficient K_T [-]:

$$K_T = \frac{H}{H_a} [-] \tag{1.2}$$

where: H – Hardness of the etalon material, respectively reference material [HRC],
H_a – Hardness of the abrasive solid [HRC] (GOST 23.208-79).

Test of resistance to abrasive wear according to the Russian standard GOST 23.208-79 was performed in the laboratories of the Technical Faculty at Czech University of Life Sciences in Prague. HARDOX 450 was chosen as an etalon sample, with which the reference sample with weld deposit OK 84.58 was compared.

The etalon and reference samples were prepared according to the standard by abrasive water jet cutting (AWJM) technology, machined by milling and grounded on a magnetic surface grinder to achieve accurate dimensions and surface roughness. OTTAWA SiO_2 silica sand with a grain size of 0.1-0.3 mm was used as abrasive solid. The hardness corresponds to the 7th degree of hardness for minerals according to Mohs scale, which corresponds to the Vickers 500 HV and Rockwell 54 HRC hardness. The test device and weighing scale is shown in Fig. 2.

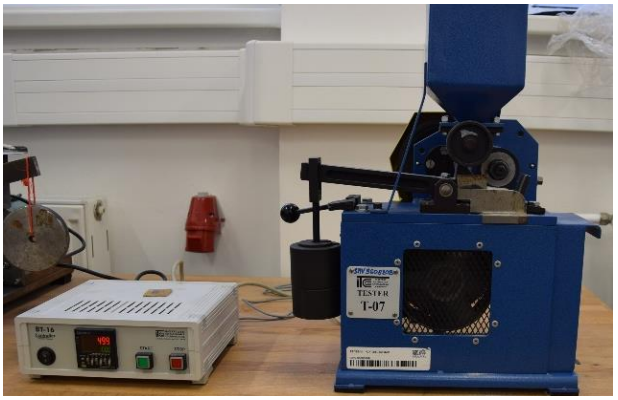

Fig. 2 The test device and weighing scale
Obr. 2 Skúšobný prístroj pre meranie oteruvzdornosti

The parameters of the test device and samples are shown in Tab. 3.

Table 3 The Parameters of the test device and samples
Tabuľka 3 Parametre skúšobného prístroja a vzoriek

The parameters of the test device[1]	
Length of the friction track in one cycle[2] R [m]	153.6
Diameter of a rubber disc[3] D [mm]	48.9
Pressing force[4] F [N]	15.48
Disc speed in one cycle[5]	1,000 ot.
Abrasive solid[6]	OTTAWA SiO_2 silica sand
The parameters of the samples[7]	
Sample size[8] [mm]	30 x 30 x 10

[1]Parametre skúšobného prístroja; [2]DÍžka trecej dráhy v jednom cykle; [3]Priemer gumeného kotúča; [4]Prítlačná sila; [5]Otáčky kolesa v jednom cykle; [6]Abrazívum; [7]Parametre vzoriek; [8]Rozmer vzorky

RESULTS AND DISCUSSION

The abrasion resistance test was firstly performed on an etalon sample. After each cycle, the etalon sample was weighed 3 times and the average weights were written in a table to determine the weight loss. The test results and weights and weight losses of HARDOX 450 are in Tab. 4.

The equation 1.2 was used to calculate the HARDOX 450 hardness coefficient K_{TE}:

$$K_{TE} = \frac{H_E}{H_A} = \frac{45}{54} = 0{,}83\ [-]$$

where: H_E – hardness of the etalon – HARDOX 450 [HRC],
H_A – hardness of the abrasive solid [HRC].

Table 4 Abrasion resistance test results– HARDOX 450
Tabuľka 4 Výsledky zo skúšky oteruvzdornosti – HARDOX 450

Track[1] R [m]	**Average weight[2] [g]**	**Weight loss[3] [g]**
0	35.3851	
153.6	35.3718	0.0133
307.2	35.3610	0.0108
460.8	35.3519	0.0091
614.4	35.3442	0.0077
768.0	35.3376	0.0066
921.6	35.3307	0.0069
1 075.2	35.3226	0.0081
1 228.8	35.3150	0.0076
1 382.4	35.3083	0.0067
1 536.0	35.3015	0.0068
1 689.6	35.2943	0.0072
	Average weight loss[4] W_{hE}	**0.0082**

[1]Dráha; [2]Priemerná hmotnosť; [3]Hmotnostný úbytok; [4]Priemerný hmotnostný úbytok

Subsequently, a test was performed on a reference sample with a weld deposit OK 84.58. After each cycle, the etalon sample was weighed 3 times and the average weights were written in a table to determine the weight loss. The test results and weights and weight losses of weld deposit OK 84.58 are in Tab. 5.

The equation 1.2 was used to calculate the weld deposit OK 84.58 hardness coefficient K_{TE}:

$$K_{TV} = \frac{H_V}{H_A} = \frac{50}{54} = 0{,}93\ [-]$$

where: H_E – hardness of the reference sample – OK 84.58 [HRC],
H_A – hardness of the abrasive solid [HRC].

Table 5 Abrasion resistance test results – OK 84.58
Tabuľka 5 Hodnoty zo skúšky oteruvzdornosti – OK 84.58

Track[1] R [m]	**Average weight[2] [g]**	**Weight loss[3] [g]**
0	35.2833	
153.6	35.2771	0.0133
307.2	35.2696	0.0108
460.8	35.2618	0.0091
614.4	35.2556	0.0077
768.0	35.2478	0.0066
921.6	34.9071	0.0069
1 075.2	35.2334	0.0081
1 228.8	35.2264	0.0076
1 382.4	35.2214	0.0067
1 536.0	35.2152	0.0068
1 689.6	35.2099	0.0072
	Average weight loss[4] W_{hR}	**0.0067**

[1]Dráha; [2]Priemerná hmotnosť; [3]Hmotnostný úbytok; [4]Priemerný hmotnostný úbytok

The test parameters and average values of weight loss of HARDOX 450 and weld deposit OK 84.58 are shown for comparison in Tab. 6.

Table 6 The abrasion resistance test – test data
Tabuľka 6 Skúška oteruvzdornosti – údaje zo skúšky

Number of cycles [-]	**Length of the friction track in one cycle[2] R [m]**	**Length of the friction track-completely[3] R [m]**	**Average weight loss[4] HARDOX 450 W_{hE} [-]**	**Average weight loss[4] OK 84.58 W_{hR} [-]**
11	153.6	1 689.6	**0.0083**	**0.0067**

[1]Počet cyklov; [2]Dĺžka trecej dráhy v jednom cykle; [3]Dĺžka trecej dráhy celkom; [4]Priemerný hmotnostný úbytok

Relative abrasion resistance was subsequently calculated according to equation 1.1:

$$\Psi_h = \frac{W_{hE}}{W_{hR}} = \frac{0.0083}{0.0067} = 1.24\ [-]$$

where: W_{hE} – weight loss of the etalon sample – HARDOX 450 [–],
W_{hR} – weight loss of the reference sample – OK 84.58 [–].

Based on the abrasive wear resistance test, we can state that the sample with the OK 84.58 weld deposit achieved 24% better resistance to abrasive wear, compared to the sample made from HARDOX 450.

CONCLUSION

Snow ploughshares are very important in terms of maintaining the passability of forest roads in winter. These roads are used to make forests accessible for heavy machinery for timber harvesting. As the ranking blades are exposed to high wear during their operation, especially abrasive, and their replacement is relatively economically demanding, it is necessary to look for ways to increase their service life and examine their resistance to abrasive wear. In further research, it would be advisable to perform a test of resistance to abrasive wear for the material of the ranking blade or ploughshares base material, as these are also exposed to the adverse effects of the working environment during their operation. Based on this test, the relative resistance to abrasive wear would be determined, where a sample with OK 84.58 weld deposit or a sample made from HARDOX 450 could be used as a reference sample. A ranking blade would be used as an etalon sample.

ACKNOWLEDGMENT

The article was supported by the APVV-16-0194 "Research on Impact of Innovation in Production Processes on the Life of Tooling and Components of Forest Mechanisms."

LITERATURE

BLAU, P.J., DEHOFF, R.R. 2013. Development of a two-body wet abrasion test method with attention to the effects of reused abradant. *Wear* 302, pp. 1035-1039. DOI:10.1016/j.wear.2012.11.040

ESAB [online]. [cit. 18-05-2021]. Available on: https://www.esab-slovakia.sk/sk/sk/products/filler-metals/repair-and-maintenance/hardfacing-alloys/ok-weartrode-55-hd.cfm

FINDIK, F. 2014. Latest progress on tribological properties of industrial materials. *Materials & Design* 57, pp. 218-244. DOI:10.1016/j.matdes.2013.12.028

GOST 23.208-79 Ensuring of wear resistance of products. Wear resistance testing of materials by friction against loosely fixed abrasive particles. [online]. [cit. 20-05-2021]. Available on: http://docs.cntd.ru/document/gost-23-208-79

HARDOX. [online]. [cit. 18-05-2021]. Available on: gamaocel.cz/4861/hardox/

SABET, H., KHIERANDISH, S., MIRDAMADI, S., GOODARZI, M. 2014. The microstructure and abrasive wear resistance of Fe-Cr-C hardfacing alloys with the composition of hypoeutectic, eutectic, and hypereutectic at Cr/C 6. *Tribology Letters* 44, pp. 237-245. DOI:10.1007/s11249-011-9842-2

SINGH, J., CHATHA, S.S., SIDHU, B.S. 2020a. Abrasive wear behavior of newly developed weld overlaid tillage tools in laboratory and in actual field conditions. *Journal of Manufacturing Processes* 55, pp. 143-152. DOI:10.1016/j.jmapro.2020.03.040

SINGH, J., CHATHA, S.S., SIDHU, B.S. 2020b. Effect of surface alloying on wear behaviour of EN-47 steel. *Materials Today Proceedings* 21, pp. 1340 – 1349. DOI: 10.1016/j.matpr.2020.01.172

SUCHÁNEK J., KUKLÍK, V., ZDRAVECKÁ E. 2009. Influence of microstructure on erosion resistance of steels. *Wear*. 267: 2092–2099. (2009). DOI:10.1016/j.wear.2009.08.004.

ŤAVODOVÁ, M., VARGOVÁ, M., FALAT, L. 2020. Possibilities of modification of ploughshares used for winter maintenance of forest roads. In Manufacturing Technology: journal for science, research and production. č. no. 6, pp. 834-844. ISSN 1213-2489

VENCL, A., MANIC, N., POPOVIC, V., MRDAK, M. 2010. Possibility of the abrasive wear resistance determination with scratch tester. *Tribology Letters* 37. pp. 591-604, DOI:10.1007/s11249-009-9556-x

VARGOVÁ, M., ŤAVODOVÁ, M. 2020. Proposal for modification of a snow ploughshare by hard surfacing to increase its service life. In Acta facultatis technicae Zvolen: scientific journal of Faculty of technology. č. č. 2, pp. 59-70. ISSN 1336-4472

ZDRAVECKÁ, E., TKÁČOVÁ, J., ONDÁČ, M. 2014. Effect of microstructure factors on abrasion resistance of high-strength steels. *Research in Agricultural Engineering* 60, pp. 115-120. ISSN 1212-9151

Corresponding author:
Ing. Monika Vargová, +421948906093, monika.vargova@is.tuzvo.sk